Parallel Solution for Per-Antenna Power Constrained Symbol-Level MU-MISO Precoding

Yunsi Wen, *Student Member, IEEE*, Junwen Yang, *Graduate Student Member, IEEE*, Ang Li, *Senior Member, IEEE*, Xuewen Liao, and Christos Masouros, *Fellow, IEEE*

***Abstract*—This paper designs a parallel solution framework for constructive interference based symbol-level precoding (CI-SLP) in the downlink of a multi-user multiple-input single-output (MU-MISO) system. Most existing works on SLP have considered the sum-power constraint, while in practical systems each transmit antenna is equipped with its dedicated power amplifier. Therefore, it is more realistic to design SLP approaches that incorporate the per-antenna power constraint (PAPC). In this paper, we focus on two specific PAPC-based problems: the constructive interference per-antenna power constraint signal to interference plus noise ratio (SINR) balancing (CI-PASB) problem and the constructive interference per-antenna peak power minimization (CI-PAPM) problem. Similar to sum-power constraint, for the CI-PASB problem, we demonstrate that it is separable, allowing the existing parallel proximal Jacobian alternating direction method of multipliers (PJ-ADMM) algorithm to be directly used. As for the CI-PAPM problem, although it is unseparable, we can leverage the established duality to obtain its solution based on the solution of the corresponding CI-PASB problem. Numerical results verify our proposed parallel methods and show that they are more efficient than the existing centralized schemes, which showcases the advantages of parallel computing and promotes the implementation of CI precoding under practical PAPC scenarios.**

***Index Terms*—MU-MISO, symbol-level precoding, per-antenna power constraint, parallel solution, optimization.**

I. Introduction

Manuscript received September 14, 2024; revised November 17, 2024; accepted February 1, 2025. This work was supported in part by the National Natural Science Foundation of China under Grant 62101422, 62371386, in part by the Young Elite Scientists Sponsorship Program by CIC (Grant No. 2021QNRC001), in part by the Science and Technology Program of Shaanxi Province under Grant 2024JC-JCQN-59, in part by the open research fund of National Mobile Communications Research Laboratory, Southeast University (No. 2024D01), and in part by the Xiaomi Young Scholars Program. The associate editor coordinating the review of this manuscript and approving it for publication was Shuangyang Li. (*Corresponding author: Ang Li.*)

Yunsi Wen and Junwen Yang are with the School of Information and Communications Engineering, Faculty of Electronic and Information Engineering, Xi'an Jiaotong University, Xi'an, Shaanxi 710049, China. (e-mail: yunsiwen@stu.xjtu.edu.cn, jwyang@stu.xjtu.edu.cn).

Ang Li is with Shaanxi Key Laboratory of Deep Space Exploration and Intelligent Information Technology, the School of Information and Communications Engineering, Faculty of Electronic and Information Engineering, Xi'an Jiaotong University, Xi'an, Shaanxi 710049, China, and is also with the National Mobile Communications Research Laboratory, Southeast University, Nanjing, China. (e-mail: ang.li.2020@xjtu.edu.cn).

Xuewen Liao is with the School of Information and Communications Engineering, Faculty of Electronic and Information Engineering, Xian Jiaotong University, Xian, Shaanxi 710049, China, and also with the National Mobile Communications Research Laboratory, Southeast University, Nanjing 210096, China. (e-mail: yeplos@mail.xjtu.edu.cn).

Christos Masouros is with the Department of Electronic and Electrical Engineering, University College London, London WC1E 7JE, U.K. (e-mail: c.masouros@ucl.ac.uk).

THE explosive growth of multimedia data traffic poses significant challenges to modern communication network architectures [1]. To address this puzzle, multiple-input multiple-output (MIMO) technology has emerged as a promising solution to enhance spectrum efficiency and improve overall system throughput. In the context of downlink transmission in multi-user multiple-input single-output (MU-MISO) systems, interference consistently hinders system performance, necessitating the development of interference management methods. In particular, it is preferable to mitigate system interference at the transmitter using transmit precoding [2]–[12], given the limited processing capabilities at the user end. While nonlinear precoding schemes such as dirty paper coding (DPC) [2], [3], Tomlinson Harashima precoding (THP) [4], [5], and vector perturbation (VP) precoding [6] can achieve optimal or near-optimal capacity performance, their complexity makes them impractical for real-world implementation. It is worth noting that both DPC and THP are designed with the idea of eliminating multi-user interference. The difference lies in that DPC achieves this through complex encoding and decoding, while THP accomplishes it through successive interference cancellation at the transmitter. Conversely, linear precoding methods are more favorable due to their closed-form nature, where the representatives include maximum ratio transmission (MRT) precoding [7], zero-forcing (ZF) precoding [8], and regularized zero-forcing (RZF) precoding [9]. Additionally, optimization-based precoding methods have garnered much attention by optimizing specific system metrics such as transmit power, signal-to-interference-plus-noise ratio (SINR), and overall throughput. Thereinto, two commonly studied problems are power minimization (PM) [10] and SINR balancing (SB) [11], [12], where the former aims to minimize total transmit power while adhering to per-user SINR constraints, while the latter focuses on maximizing the minimum SINR among all users under total power constraint.

In the aforementioned precoding schemes, interference in the system is constantly considered as a disadvantageous factor, which is to be eliminated. However, recent research has presented a new perspective on interference by using symbol-level precoding (SLP) to control instantaneous interference and leverage it as effective power [13]–[15]. In the literature of SLP, the concept of constructive interference (CI) and destructive interference (DI) is firstly introduced in [16]. [17] proposes a partial channel inversion method to eliminate DI while preserving CI. Furthermore, in [18], the phase of the received symbol is rotated to align with the phase of the desired signal, thereby transforming DI into CI within the

system. The 'phase rotation' metric for PSK signaling is introduced in [19], where the CI condition is further relaxed, and the concept of 'constructive interference region' is presented. Moreover, [20] introduces the 'symbol-scaling' metric to exploit interference under QAM signaling, where only the outer constellation points can be utilized for interference exploitation. We note that, compared to DPC and THP, the design philosophy of CI precoding is to exploit multi-user interference, rather than eliminating interference as in DPC and THP. However, we note that, CI-based approahes require symbol-by-symbol precoding, which thus brings challenges to its application and necessitates the development of efficient and low-complexity solutions [19], [21]–[29]. In [19], by leveraging the virtual multicast formulation and Lagrangian duality, the constructive interference power minimization (CI-PM) problem can be transformed into a non-negative least-squares problem, which is then addressed using the efficient gradient projection algorithm. Building upon this non-negative least-squares problem, [21] proposes a sub-optimal closed-form solution to further reduce the complexity of solving CI-PM problem. Furthermore, distinct from the centralized solutions in [19] and [21], [22] introduces the parallel inverse-free (PIF) method to address the CI-PM problem, where the time complexity is greatly reduced by adopting the parallel computing framework. For the constructive interference SINR balancing (CI-SB) problem, [23] and [24] propose the closed-form iterative precoders under PSK and QAM, respectively. It is worth noting that the iterations converge within a few steps, effectively reducing the complexity of solving CI-SB problem. In [25], a block-level CI-SB scheme is proposed, where the transmit symbols over multiple slots are jointly considered to decrease the update rate of the precoding matrix and further reduce the complexity of CI precoding. Moreover, [26] establishes the duality between the CI-PM problem and the CI-SB problem, enabling the methods for solving the CI-PM problem to be utilized for solving its CI-SB counterpart, and vice versa. In addition to the aforementioned traditional optimization-based methods, deep learning-based methods can also be applied to reduce the complexity of CI precoding [27]–[29].

It should be emphasized that the CI precoding schemes discussed above consider the sum-power constraint (SPC), which may not be practical in real scenarios where each transmit antenna has its dedicated power amplifier [30]–[32]. Therefore, designing CI-based precoders under per-antenna power constraint (PAPC) is more realistic in practical applications [33]–[37]. In [33], the peak power minimization problem subject to individual SINR constraints is studied using the 'strict phase rotation' metric of CI precoding. [34] proposes the CI-based SINR balancing problem under PAPC, which is shown to be the inverse problem of the problem in [33]. Based on the inverse property, a bi-section method is presented to solve the proposed SINR balancing problem. In [35], the weighted per-antenna power minimization problem and the spatial peak-to-average power ratio (SPAPR) minimization problem are presented with the 'strict phase rotation' metric, respectively. Since these two problems are both non-convex, with the aid of successive convex approximation (SCA) framework, [35] approximates the original problems into multiple solvable convex problems and solves them sequentially. Furthermore, for the CI-SB problem under PAPC, [36] proposes the unified projected gradient (PG) framework to solve both strict and non-strict cases with the 'phase rotation' metric. However, the approximation procedure in [36] results in a sub-optimal solution. [37] introduces the optimal precoder structure for the CI-SB problem under PAPC, which serves as a generalized version of the CI-SB precoding matrix under SPC (the one that is proposed in [23]). It is noteworthy that the above literature on PAPC-based approaches primarily focuses on centralized schemes, which can become overly complex as the number of antennas in the system grows, resulting in higher-dimensional matrix operations. To effectively address this challenge, a practical strategy is to design PAPC precoders in a parallel fashion, which is the primary focus of this paper. It is important to highlight that, by utilizing parallel decomposition, we can significantly reduce the dimension of optimization variables, leading to a notable decrease in complexity.

In this paper, different from the existing centralized schemes, we propose parallel solutions to two CI-based problems: the constructive interference per-antenna power constraint SINR balancing (CI-PASB) problem and the constructive interference per-antenna peak power minimization (CI-PAPM) problem, where the phase rotation metric is used for PSK modulation while the symbol scaling metric is adopted for QAM modulation. The main contributions of our study are as follows:

1) Regarding the precoder design under PSK signaling, we formulate the CI-PASB problem and CI-PAPM problem with the more general 'non-strict phase rotation' metric. For the CI-PASB problem, we derive its separable equivalence by adjusting the order of elements in the optimization variables, and hence the existing parallel proximal Jacobian alternating direction method of multipliers (PJ-ADMM) algorithm can be directly employed [38]. Additionally, in the above PJ-ADMM iterations, we prove that each subproblem has a closed-form solution, thereby avoiding the need for inner iterations and further reducing the complexity of the entire parallel algorithm.
2) As for the unseparable CI-PAPM problem under PSK, we cannot handle it using existing parallel methods. However, according to the duality [26] between the CI-PM problem and the CI-SB problem, similarly we can establish the duality between the CI-PAPM problem and the CI-PASB problem. Such duality allows us to obtain the solution for the CI-PAPM problem by leveraging the solution of its CI-PASB counterpart, and vice versa. Therefore, we can use the same PJ-ADMM framework to tackle the CI-PAPM problem.
3) We extend the above parallel solutions to QAM modulation, where the CI design metric becomes symbol scaling metric. We note that, with a minor modification, the PJ-ADMM framework designed for PSK modulation can readily be extended to QAM modulation. Moreover, we can demonstrate that the duality between these two problems remains unchanged, and hence we can exploit

the existing duality to tackle the CI-PAPM problem under QAM as well.

From the numerical results, it is evident that the proposed parallel PJ-ADMM algorithm is effective in solving both the CI-PASB and CI-PAPM problems, which not only validates the derived formulas and established duality, but also highlights the notable efficiency of the parallel algorithm. It is worth noting that the proposed method can achieve near-optimal results within just tens of iterations, while maintaining computational complexity that is almost identical to that of the closed-form ZF-PAPC precoder.

The remainder of this paper is organized as follows. Section II introduces the MU-MISO system model, along with the concept of constructive interference. Section III focuses on presenting the parallel solutions under PSK. In Section IV, we extend the parallel solutions to QAM signaling. In Section V, we evaluate the complexity of our proposed PJ-ADMM framework. Finally, we present the numerical results in Section VI and conclude this paper in Section VII.

Notation: a, $\mathbf{a}$, and $\mathbf{A}$ represent a scalar, column vector, and matrix, respectively. The set of $l \times l$ complex (real) matrices is denoted as $\mathbb{C}^{l\times l}$ ($\mathbb{R}^{l\times l}$). $(\cdot)^H$, $(\cdot)^T$, and $(\cdot)^{-1}$ denote conjugate transposition, transposition, and inverse, respectively. $\Re(\cdot)$ ($\Im(\cdot)$) represents the real (imaginary) part of an element. $|\cdot|$ denotes the absolute value of a number, and $\|\cdot\|$ signifies the norm of a vector or matrix. Additionally, we note that $\|\mathbf{x}\|_{\mathbf{A}}^2 = \mathbf{x}^H\mathbf{A}\mathbf{x}$. We use $\mathbf{e}_j$ to denote the j-th column of the identity matrix, and $\mathbf{0}$ represents the zero vector. $\hat{\mathbf{x}}^{PM*}(\mathbf{b})$ denotes the optimal solution of the CI-PAPM problem given the input $\mathbf{b}$, and $\hat{\mathbf{x}}^{SB*}(\mathbf{b}, P)$ denotes the optimal solution of the CI-PASB problem given the input $\mathbf{b}$ and P.

II. System Model

A. MU-MISO System Model

We investigate a MU-MISO system with N_t transmit antennas and K single-antenna users, and the downlink transmission procedure can be formulated as

$$\mathbf{r} = \mathbf{H}\mathbf{x} + \mathbf{n}. \tag{1}$$

$\mathbf{x} = [x_1, \cdots, x_{N_t}]^T \in \mathbb{C}^{N_t\times 1}$ is the transmitted signal vector from N_t antennas, $\mathbf{H} = [\mathbf{h}_1, \cdots, \mathbf{h}_K]^T \in \mathbb{C}^{K\times N_t}$ is the channel matrix, $\mathbf{n} = [n_1, \cdots, n_K]^T \in \mathbb{C}^{K\times 1}$ is the complex Gaussian noise vector with zero-mean and variance σ^2 per entry, and $\mathbf{r} = [r_1, \cdots, r_K]^T \in \mathbb{C}^{K\times 1}$ is the received signal vector for all users. To handle the multi-user interference (MUI), modulated M-PSK (or M-QAM) symbol vector $\mathbf{s} = [s_1, \cdots, s_K]^T \in \mathbb{C}^{K\times 1}$ needs to pass through the precoder matrix $\mathbf{W} = [\mathbf{w}_1, \cdots, \mathbf{w}_K] \in \mathbb{C}^{N_t\times K}$, i.e., $\mathbf{x} = \mathbf{W}\mathbf{s}$. Throughout this paper, we assume perfect channel state information (CSI) is provided at the transmitter for precoding design.

B. Constructive Interference

In the downlink of MU-MISO transmission, multi-user interference in the spatial domain on the same time-frequency resource is a critical factor that limits system performance. In traditional precoding schemes, this interference is viewed as an undesirable factor and is minimized as much as possible. In contrast, the symbol-level precoding scheme based on constructive interference (CI), which this paper discusses, takes a different perspective on interference. Specifically, CI precoding divides the multi-user interference present in the system into CI and destructive interference (DI). CI refers to interference that pushes the received constellation points away from the detection boundaries, while DI refers to interference that pulls the received constellation points closer to the detection threshold, which is detrimental to detection at the receiver. Next, we will start from model (1) to further explain the concepts of CI and DI. In the system model (1), the received symbol at user i can be expressed as

$$r_i = \mathbf{h}_i^T\mathbf{w}_i s_i + \mathbf{h}_i^T \sum_{j,j\neq i} \mathbf{w}_j s_j + n_i, \tag{2}$$

where the first term $\mathbf{h}_i^T\mathbf{w}_i s_i$ represents the desired signal, and the second term represents the interference signal. It should be noted that the interference term in (2) can be constructive or destructive, depending on whether the interference signal is beneficial to detection at the receiver end. Specifically, if the superposition of the interference signal causes the constellation points at the receiver end to move further away from the detection boundaries, then such interference signal is considered constructive. Otherwise, it is considered destructive. Based on the above analysis, the goal of CI precoding is to transform the interfering signal $\mathbf{h}_i^T \sum_{j,j\neq i} \mathbf{w}_j s_j$ into useful signal power. This differs from traditional precoding design, where the interference term is always considered harmful. For details regarding specific interference exploitation methods, various metrics are utilized to convert overall interference into constructive interference, depending on the modulation types employed. For example, we use the phase rotation metric for PSK signaling and the symbol scaling metric for QAM signaling. In the following two sections, we will introduce the CI precoding design under PSK modulation and QAM modulation, providing detailed explanations of these two metrics.

III. Parallel Solutions for CI-PASB Problem and CI-PAPM Problem with PSK Signaling

In this section, parallel methods are proposed to address the constructive interference per-antenna power constraint SINR balancing (CI-PASB) problem and the constructive interference per-antenna peak power minimization (CI-PAPM) problem with PSK signaling. Firstly, we will introduce the phase rotation metric of CI precoding, followed by the formulations of these two problems. We then establish the duality between the CI-PASB problem and the CI-PAPM problem, which links the solutions to these two problems. We further observe that, the CI-PASB problem can be transformed into a separable version by utilizing a permutation matrix, allowing us to directly employ the parallel proximal Jacobian alternating direction method of multipliers (PJ-ADMM) algorithm introduced in [38]. Furthermore, although the CI-PAPM problem inherently lacks separability, we can utilize the established duality to

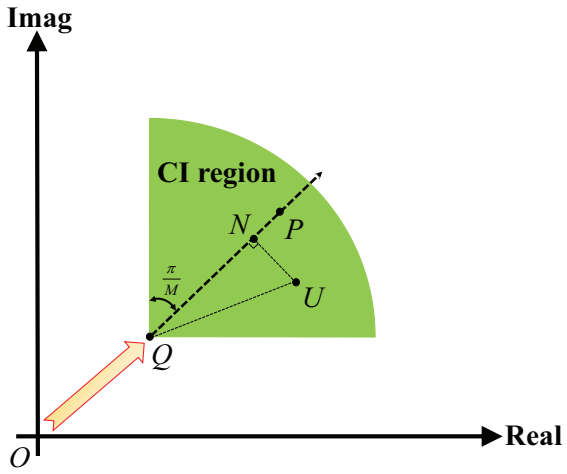

Fig. 1: Phase rotation metric for PSK signaling, QPSK.
Notes: $|\vec{OQ}| = t$, $|\vec{ON}| = \Re(\lambda_k)$, $|\vec{OU}| = |\lambda_k|$, $|\vec{UN}| = |\Im(\lambda_k)|$.

convert its solution into the solution of the corresponding CI-PASB problem, and hence it can be solved within the same PJ-ADMM framework.

A. Phase Rotation Metric and Problem Formulations

For PSK signaling examined in this section, the associated CI design metric is the 'phase rotation' metric. The schematic diagram of that is illustrated in Fig. 1, where the received noiseless signal at user k is restricted to this green CI region given the desired normalized symbol $s_k = \frac{\sqrt{2}}{2} + j \cdot \frac{\sqrt{2}}{2}$. The CI region in Fig. 1 refers to the area formed by all the received constellation points after CI precoding. When the constellation points lie within the CI region, their distances to all detection thresholds are increased compared with the nominal constellation point, thereby improving the detection performance. For a more detailed explanation, phase rotation metric can be further categorized into strict and non-strict cases. In Fig. 1, constellation point P conforms to the strict phase rotation metric, i.e., the phase of P is strictly aligned with that of s_k. As a more relaxed version, non-strict phase rotation does not require this kind of alignment, and the received symbol only needs to stay in the CI region (such as constellation point U in Fig. 1). Constellation point Q is the vertex of the CI region, and its distance from the origin can be expressed as t, which is also the objective to be maximized in CI precoding. Moreover, N is an auxiliary point introduced for modeling the non-strict phase rotation metric, defined as the projection of constellation point U onto $\vec{PQ}$, i.e., $\angle UNQ = \frac{\pi}{2}$. Without loss of generality, we consider the more general non-strict phase rotation metric in the following precoder design. Specifically, the CI conditions for user k are given by

$$\mathbf{h}_k^T \mathbf{W}\mathbf{s} - \lambda_k s_k = 0, \tag{3}$$

$$|\Im(\lambda_k)| - (\Re(\lambda_k) - t)\tan(\pi/M) \leq 0, \tag{4}$$

where λ_k is complex forcing the received symbol stay in the CI region, and t is the measure of distance between CI region and detection boundaries. As an explanation of (4), we note that the condition that the constellation point U needs to satisfy to stay in CI region is

$$\begin{aligned} \angle UQN \leq \pi/M &\Rightarrow^1 \tan(\angle UQN) \leq \tan(\pi/M) \\ &\Rightarrow^2 \frac{|\vec{UN}|}{|\vec{ON}| - |\vec{OQ}|} \leq \tan(\pi/M) \\ &\Rightarrow^3 \frac{|\Im(\lambda_k)|}{\Re(\lambda_k) - t} \leq \tan(\pi/M), \end{aligned} \tag{5}$$

where the transformation denoted by $\Rightarrow^1$ follows from the fact that $M \geq 2$. The transformation $\Rightarrow^2$ is based on the relation $\tan(\angle UQN) = |\vec{UN}|/|\vec{QN}|$, where $|\vec{QN}| = |\vec{ON}| - |\vec{OQ}|$. Furthermore, based on (3), in Fig. 1 we represent the vector $\vec{OU}$ as $\lambda_k s_k$, the vector $\vec{ON}$ as $\Re(\lambda_k)s_k$, the vector $\vec{UN}$ as $j \cdot \Im(\lambda_k)s_k$, and the vector $\vec{OQ}$ as $t \cdot s_k$. Since $|s_k| = 1$, the transformation $\Rightarrow^3$ follows naturally, from which we obtain (4).

Next, we will elaborate on the formulations of the CI-PASB problem and the CI-PAPM problem. Before that, we need to formulate the SINR constraints firstly. Since the MUI is utilized in CI precoding, the actual system becomes interference-free and the SINR expression for user k is $\frac{|\mathbf{h}_k^T \mathbf{W}\mathbf{s}|^2}{\sigma^2}$. With a predefined boundary γ_k, the SINR constraints can be directly derived as

$$\frac{|\mathbf{h}_k^T \mathbf{W}\mathbf{s}|^2}{\sigma^2} \geq \gamma_k, \quad \forall k \in \{1, \cdots, K\}. \tag{6}$$

Nevertheless, the formulation (6) is non-convex and hence some transformations are needed to handle it, such as the method in [33]. To avoid such cumbersome constraints, it is worth noting that we can employ the definition of CI region to construct SINR constraints. Specifically, in Fig. 1, the vertex Q of CI region owns the minimum SINR among all received symbols, and thus the relationship between t and γ_k can be established as $t = \sqrt{\gamma_k}\sigma$. Then, we define $\tilde{\mathbf{h}}_k^T = \frac{\mathbf{h}_k^T}{s_k}$ and rewrite (3) as $\lambda_k = \tilde{\mathbf{h}}_k^T \mathbf{x}$. By substituting $\lambda_k = \tilde{\mathbf{h}}_k^T \mathbf{x}$ and $t = \sqrt{\gamma_k}\sigma$ into (4), the SINR constraint and CI constraint for user k can be combined as

$$\Re(\tilde{\mathbf{h}}_k^T \mathbf{x}) - \frac{|\Im(\tilde{\mathbf{h}}_k^T \mathbf{x})|}{\tan(\pi/M)} \geq \sqrt{\gamma_k}\sigma. \tag{7}$$

We can observe that expression (7) is convex and effectively captures both the CI constraint and the SINR constraint, surpassing the non-convex formulations proposed in [33], [34].

To proceed with (7), we can construct the constructive interference per-antenna peak power minimization (CI-PAPM) problem as below

$$\begin{aligned} &\min_{\mathbf{x}} \max_{i} \ |x_i|^2 \\ &s.t. \ \Re(\tilde{\mathbf{h}}_k^T \mathbf{x}) - \frac{|\Im(\tilde{\mathbf{h}}_k^T \mathbf{x})|}{\tan(\pi/M)} \geq \sqrt{\gamma_k}\sigma, \ \forall k \in \{1, \cdots, K\}, \end{aligned} \tag{8}$$

where in order to decrease the variable dimension we optimize $\mathbf{x}$ instead of $\mathbf{W}$. Then, by introducing an auxiliary variable

$u \in \mathbb{R}$, problem (8) is equivalent to

$$\begin{aligned} &\min_{\mathbf{x},u} \ u \\ &s.t. \ |x_i|^2 \le u, \ \forall i \in \{1,\cdots,N_t\}, \\ &\quad \Re(\tilde{\mathbf{h}}_k^T\mathbf{x}) - \frac{\left|\Im(\tilde{\mathbf{h}}_k^T\mathbf{x})\right|}{\tan(\pi/M)} \ge \sqrt{\gamma_k}\sigma, \ \forall k \in \{1,\cdots,K\}. \end{aligned} \quad (9)$$

Furthermore, with $\hat{\mathbf{x}} = \begin{bmatrix}\Re(\mathbf{x})\\ \Im(\mathbf{x})\end{bmatrix}$, $\mathbf{N} = \begin{bmatrix}1 & -\frac{1}{\tan(\pi/M)}\\ 1 & \frac{1}{\tan(\pi/M)}\end{bmatrix}$, $\mathbf{S}_k = \begin{bmatrix}\Re(\frac{1}{s_k}) & -\Im(\frac{1}{s_k})\\ \Im(\frac{1}{s_k}) & \Re(\frac{1}{s_k})\end{bmatrix}$, $\mathbf{H}_k = \begin{bmatrix}\Re(\mathbf{h}_k^T) & -\Im(\mathbf{h}_k^T)\\ \Im(\mathbf{h}_k^T) & \Re(\mathbf{h}_k^T)\end{bmatrix}$, $\mathbf{A}_k = \mathbf{N}\mathbf{S}_k\mathbf{H}_k$, $\mathbf{b}_k = \sqrt{\gamma_k}\sigma \cdot \mathbf{1}$, $\mathbf{A} = [\mathbf{A}_1^T,\cdots,\mathbf{A}_K^T]^T$, $\mathbf{b} = [\mathbf{b}_1^T,\cdots,\mathbf{b}_K^T]^T$ and $\mathbf{E}_j = \mathbf{e}_j\mathbf{e}_j^T + \mathbf{e}_{j+N_t}\mathbf{e}_{j+N_t}^T$, (9) can be transformed into a real-valued optimization problem

$$\begin{aligned} &\min_{\hat{\mathbf{x}},u} \ u \\ &s.t. \mathbf{A}\hat{\mathbf{x}} \succeq \mathbf{b} \\ &\quad \hat{\mathbf{x}}^T\mathbf{E}_j\hat{\mathbf{x}} \le u, \ \forall j \in \{1,\cdots,N_t\}. \end{aligned} \quad (10)$$

Similarly, given the peak power boundary P, the constructive interference per-antenna power constraint SINR balancing (CI-PASB) problem can be formulated as follows

$$\begin{aligned} &\max_{\mathbf{x},q} \ q \\ &s.t. \ |x_i|^2 \le P, \ \ \forall i \in \{1,\cdots,N_t\}, \\ &\quad \Re(\tilde{\mathbf{h}}_k^T\mathbf{x}) - \frac{\left|\Im(\tilde{\mathbf{h}}_k^T\mathbf{x})\right|}{\tan(\pi/M)} \ge q\cdot\sqrt{\gamma_k}\sigma, \ \forall k \in \{1,\cdots,K\}, \end{aligned} \quad (11)$$

and its real-valued counterpart is

$$\begin{aligned} &\max_{\hat{\mathbf{x}},q} \ q \\ &s.t. \mathbf{A}\hat{\mathbf{x}} \succeq q\cdot\mathbf{b} \\ &\quad \hat{\mathbf{x}}^T\mathbf{E}_j\hat{\mathbf{x}} \le P, \ \forall j \in \{1,\cdots,N_t\}. \end{aligned} \quad (12)$$

It is worth noting that in the CI-PASB problem, the expression for t is no longer $t = \sqrt{\gamma_k}\sigma$, but rather $t = q\cdot\sqrt{\gamma_k}\sigma$ because the signals have passed through the wireless channel, where q is the introduced scaling factor. At first glance, it appears that both (10) and (12) are unseparable problems, making them unsuitable for existing parallel approaches[1]. However, in the later subsection, we will demonstrate that problem (12) can be made separable by rearranging the entries of vector $\hat{\mathbf{x}}$.

B. Duality Between CI-PASB and CI-PAPM

Before introducing the parallel solutions to the CI-PASB problem and the CI-PAPM problem, we first demonstrate the duality between these two problems, which will establish a connection between their solutions and facilitate the design of subsequent parallel algorithms.

[1]In general, parallel methods can only be employed to solve optimization problems that can be formulated in separable forms. For unseparable problems, direct application of parallel algorithms is often challenging, thus necessitating a transformation of their formulations.

Proposition 1: Given the CI-PAPM problem with input $\mathbf{b}$ and output $(u^*, \hat{\mathbf{x}}^{PM*})$, the solution of the corresponding CI-PASB problem with input $(\mathbf{b}, P)$ can be obtained as

$$q^* = \sqrt{\frac{P}{u^*}}, \quad \hat{\mathbf{x}}^{SB*} = q^*\cdot\hat{\mathbf{x}}^{PM*}. \quad (13)$$

Similarly, considering the CI-PASB problem with input $(\mathbf{b}, P)$ and output $(q^*, \hat{\mathbf{x}}^{SB*})$, the solution of its CI-PAPM counterpart with input $\mathbf{b}$ is

$$u^* = \frac{P}{(q^*)^2}, \quad \hat{\mathbf{x}}^{PM*} = \hat{\mathbf{x}}^{SB*}/q^*. \quad (14)$$

Proof: Firstly, with the contradiction method in [12], it is trivial to demonstrate that (10) and (12) are inverse problems, and thus the following equations hold true[2]:

$$\hat{\mathbf{x}}^{PM*}(\alpha\mathbf{b}) = \hat{\mathbf{x}}^{SB*}(\mathbf{b}, u^*(\alpha\mathbf{b})), \quad \alpha = q^*(\mathbf{b}, u^*(\alpha\mathbf{b})). \quad (15)$$

$$\hat{\mathbf{x}}^{SB*}(\mathbf{b}, P) = \hat{\mathbf{x}}^{PM*}(q^*(\mathbf{b}, P)\mathbf{b}), P = u^*(q^*(\mathbf{b}, P)\mathbf{b}). \quad (16)$$

Then, by substituting $\hat{\mathbf{x}} = \frac{1}{\beta}\tilde{\mathbf{x}}$ into (10), the scaling property of CI-PAPM problem can be expressed as

$$\hat{\mathbf{x}}^{PM*}(\beta\cdot\mathbf{b}) = \beta\cdot\hat{\mathbf{x}}^{PM*}(\mathbf{b}), \ u^*(\beta\cdot\mathbf{b}) = \beta^2\cdot u^*(\mathbf{b}). \quad (17)$$

Given the aforementioned characteristics of inverse problems and the scaling property, we will further elaborate on the procedure for proving duality. Specifically, according to (15) and (17), we have

$$\begin{aligned} \hat{\mathbf{x}}^{SB*}(\mathbf{b}, P) &= \hat{\mathbf{x}}^{SB*}(\mathbf{b}, \frac{P}{u^*(\mathbf{b})}\cdot u^*(\mathbf{b})) \\ &= \hat{\mathbf{x}}^{SB*}(\mathbf{b}, u^*(\sqrt{\frac{P}{u^*(\mathbf{b})}}\cdot\mathbf{b})) \\ &= \hat{\mathbf{x}}^{PM*}(\sqrt{\frac{P}{u^*(\mathbf{b})}}\cdot\mathbf{b}) \\ &= \sqrt{\frac{P}{u^*(\mathbf{b})}}\cdot\hat{\mathbf{x}}^{PM*}(\mathbf{b}). \end{aligned} \quad (18)$$

Moreover, with (16) and (17), we can obtain

$$P = u^*(q^*(\mathbf{b}, P)\mathbf{b}) = (q^*(\mathbf{b}, P))^2\cdot u^*(\mathbf{b}) = (q^*)^2\cdot u^*, \quad (19)$$

and then (18) can be further transformed into

$$\hat{\mathbf{x}}^{SB*}(\mathbf{b}, P) = q^*\cdot\hat{\mathbf{x}}^{PM*}(\mathbf{b}) = q^*\cdot\hat{\mathbf{x}}^{PM*}. \quad (20)$$

Consequently, we have successfully demonstrated the validity of equation (13), and equation (14) can be proven using the same approach. To maintain conciseness, we refrain from detailing the process here. ■

The duality presented in ***Proposition 1*** highlights the fact that the solution to the CI-PAPM problem can be obtained by addressing its counterpart CI-PASB problem, and vice versa. However, it is advisable to initially tackle the one that is more manageable within the two problems and then utilize the established duality to handle the other one. Therefore, considering the motivation for parallel processing and the

[2]The specific proofs for (15) and (16) follow a methodology similar to that of **Lemma 1** in [26]. Therefore, we will refrain from further elaboration here for the sake of brevity.

unseparable nature of the CI-PAPM problem, we will now concentrate on the parallel solution of the CI-PASB problem that is separable.

C. Parallel Solution for CI-PASB Problem

As the expression (12) of the CI-PASB problem remains unseparable, we need to reconstruct it into a separable form firstly. Letting $\mathbf{c} = [0, 0, \cdots, 1]^T$, $\hat{\mathbf{c}} = [0, 0, \cdots, -1]^T$, $\mathbf{E} = \begin{bmatrix} \mathbf{I} & \mathbf{0} \end{bmatrix}$, $\mathbf{y} = [\hat{\mathbf{x}}^T, q]^T$, $q = \mathbf{c}^T\mathbf{y}$, $\hat{\mathbf{x}} = \mathbf{E}\mathbf{y}$, $\hat{\mathbf{A}} = \mathbf{A}\mathbf{E} - \mathbf{b}\mathbf{c}^T$ and $\hat{\mathbf{E}}_j = \mathbf{E}^T\mathbf{E}_j\mathbf{E}$, the original problem (12) is equivalent to

$$\begin{aligned} &\min_{\mathbf{y}} \ \hat{\mathbf{c}}^T\mathbf{y} \\ &s.t. \ \hat{\mathbf{A}}\mathbf{y} \succeq \mathbf{0} \\ &\quad \mathbf{y}^T\hat{\mathbf{E}}_j\mathbf{y} \leq P, \ \forall j \in \{1, \cdots, N_t\}. \end{aligned} \tag{21}$$

Next, we introduce a permutation matrix $\mathbf{G}$ to rearrange the entries of $\mathbf{y}$ as follows

$$\begin{bmatrix} x_1^{\Re} \\ x_1^{\Im} \\ \vdots \\ x_{N_t}^{\Re} \\ x_{N_t}^{\Im} \\ q \end{bmatrix} = \begin{bmatrix} 1 & 0 & \cdots & 0 & 0 & 0 & \cdots & 0 & 0 \\ 0 & 0 & \cdots & 0 & 1 & 0 & \cdots & 0 & 0 \\ \vdots & \vdots & \vdots & \vdots & \vdots & \vdots & \vdots & \vdots & \vdots \\ 0 & 0 & \cdots & 1 & 0 & 0 & \cdots & 0 & 0 \\ 0 & 0 & \cdots & 0 & 0 & 0 & \cdots & 1 & 0 \\ 0 & 0 & \cdots & 0 & 0 & 0 & \cdots & 0 & 1 \end{bmatrix} \cdot \begin{bmatrix} x_1^{\Re} \\ x_2^{\Re} \\ \vdots \\ x_{N_t-1}^{\Im} \\ x_{N_t}^{\Im} \\ q \end{bmatrix}$$
$$\mathbf{z} = \mathbf{G} \cdot \mathbf{y}, \tag{22}$$

where we note that $\mathbf{y} = [x_1^{\Re}, x_2^{\Re}, \cdots, x_{N_t-1}^{\Im}, x_{N_t}^{\Im}, q]^T$, $\mathbf{z} = [x_1^{\Re}, x_1^{\Im}, \cdots, x_{N_t}^{\Re}, x_{N_t}^{\Im}, q]^T$, and $x_i^{\Re}$ ($x_i^{\Im}$) denotes the real (imaginary) part of the signal from the i-th transmit antenna. Since $\mathbf{G}$ is invertible, we substitute $\mathbf{y} = \mathbf{G}^{-1}\mathbf{z}$ into (21) and obtain the problem regarding variable $\mathbf{z}$ as

$$\begin{aligned} &\min_{\mathbf{z}} \ \tilde{\mathbf{c}}^T\mathbf{z} \\ &s.t. \ \tilde{\mathbf{A}}\mathbf{z} \succeq \mathbf{0} \\ &\quad \mathbf{z}^T\tilde{\mathbf{E}}_j\mathbf{z} \leq P, \ \forall j \in \{1, \cdots, N_t\}, \end{aligned} \tag{23}$$

where $\tilde{\mathbf{c}} = \hat{\mathbf{c}}$, $\tilde{\mathbf{A}} = \hat{\mathbf{A}}\mathbf{G}^{-1}$, and $\tilde{\mathbf{E}}_j = (\mathbf{G}^{-1})^T\hat{\mathbf{E}}_j\mathbf{G}^{-1}$. Furthermore, we split $\mathbf{z}$ into N blocks, i.e., $\mathbf{z} = [\mathbf{z}_1^T, \cdots, \mathbf{z}_N^T]^T$, where each $\mathbf{z}_i$ owns n_i entries and hence $\sum_{i=1}^N n_i = 2N_t + 1$. In order to obtain a separable version, considering the per-antenna power constraints in (23), the real and imaginary parts of the signal from the same transmit antenna must be placed in the same block. Then, without loss of generality we assume that each block has an equal number of elements, with the exception of the last block $\mathbf{z}_N$ which includes an additional variable q (i.e., $\mathbf{z}_{i, i\neq N}$ owns $\frac{2N_t}{N}$ elements, while $\mathbf{z}_N$ owns $\frac{2N_t}{N} + 1$ elements). Given the aforementioned descriptions, the separable equivalence of (23) can be expressed as

$$\begin{aligned} &\min_{\mathbf{z}_i \in \chi_i} \ \sum_{i=1}^N \tilde{\mathbf{c}}_i^T\mathbf{z}_i \\ &s.t. \ \sum_{i=1}^N \tilde{\mathbf{A}}_i\mathbf{z}_i \succeq \mathbf{0}, \end{aligned} \tag{24}$$

where $\tilde{\mathbf{c}} = [\tilde{\mathbf{c}}_1^T, \cdots, \tilde{\mathbf{c}}_N^T]^T$, $\tilde{\mathbf{A}} = [\tilde{\mathbf{A}}_1, \cdots, \tilde{\mathbf{A}}_N]$, and $\chi_i = \left\{\mathbf{z}_i \mid \mathbf{z}_i^T\mathbf{F}_{i,j}\mathbf{z}_i \leq P, \ j = 1, \cdots, \frac{N_t}{N}\right\}$. Regarding $\mathbf{F}_{i,j}$, it should be noted that each $\mathbf{F}_{i,j}$ in χ_i has two 1s on the diagonal while the other entries are 0, which enables the extraction of the real and imaginary parts of the transmitted signal on the j-th antenna.

With the reformulated expression (24), we can conveniently address the CI-PASB problem in a parallel manner. We point out that, there are various types of parallel algorithms available for addressing problem (24) [38]–[40]. In this paper, we opt to employ a relatively efficient parallel algorithm based on ADMM, namely the PJ-ADMM algorithm, as detailed below [38]. Firstly, by introducing $\mathbf{m} = \sum_{i=1}^N \tilde{\mathbf{A}}_i\mathbf{z}_i$ and the indicator function

$$I(\mathbf{m}) = \begin{cases} 0, & if \ \mathbf{m} \succeq \mathbf{0} \\ \infty, & otherwise \end{cases} \tag{25}$$

problem (24) can be transformed into

$$\begin{aligned} &\min_{\mathbf{m}, \ \mathbf{z}_i \in \chi_i} \ \sum_{i=1}^N \tilde{\mathbf{c}}_i^T\mathbf{z}_i + I(\mathbf{m}) \\ &\quad s.t. \ \mathbf{m} = \sum_{i=1}^N \tilde{\mathbf{A}}_i\mathbf{z}_i. \end{aligned} \tag{26}$$

Then, using the penalty parameter $\rho > 0$ and the Lagrangian multiplier $\boldsymbol{\lambda}$, we can express the augmented Lagrangian of (26) as follows

$$\begin{aligned} \mathcal{L}_{aug} = &\sum_{i=1}^N \tilde{\mathbf{c}}_i^T\mathbf{z}_i + I(\mathbf{m}) \\ &+ \boldsymbol{\lambda}^T \cdot (\mathbf{m} - \sum_{i=1}^N \tilde{\mathbf{A}}_i\mathbf{z}_i) + \frac{\rho}{2}\left\|\mathbf{m} - \sum_{i=1}^N \tilde{\mathbf{A}}_i\mathbf{z}_i\right\|_2^2. \end{aligned} \tag{27}$$

To facilitate subsequent derivations, we express (27) in a more convenient form, which is given by

$$\begin{aligned} \mathcal{L}_{aug} = &\sum_{i=1}^N \tilde{\mathbf{c}}_i^T\mathbf{z}_i + I(\mathbf{m}) \\ &+ \frac{\rho}{2}\left\|\mathbf{m} - \sum_{i=1}^N \tilde{\mathbf{A}}_i\mathbf{z}_i + \frac{\boldsymbol{\lambda}}{\rho}\right\|_2^2 - \frac{1}{2\rho}\left\|\boldsymbol{\lambda}\right\|_2^2. \end{aligned} \tag{28}$$

According to the PJ-ADMM framework [38], during the n-th iteration, the parallel ADMM procedure consists of the following three updates:

1) Update of $\mathbf{m}^{n+1}$:

$$\mathbf{m}^{n+1} = \underset{\mathbf{m}}{\operatorname{argmin}} \ \mathcal{L}_{aug}(\mathbf{z}_{i,i=1,\cdots,N}^n, \mathbf{m}, \boldsymbol{\lambda}^n) \tag{29}$$

2) Update of $\mathbf{z}_i^{n+1}$ (parallel):

$$\mathbf{z}_i^{n+1} = \underset{\mathbf{z}_i \in \chi_i}{\operatorname{argmin}} \ \mathcal{L}_{aug}(\mathbf{z}_i, \mathbf{z}_{j,j\neq i}^n, \mathbf{m}^{n+1}, \boldsymbol{\lambda}^n) + \frac{1}{2}\left\|\mathbf{z}_i - \mathbf{z}_i^n\right\|_{\mathbf{P}_i}^2 \tag{30}$$

3) Update of $\boldsymbol{\lambda}^{n+1}$:

$$\boldsymbol{\lambda}^{n+1} = \boldsymbol{\lambda}^n + \hat{\gamma}\rho \cdot (-\sum_{i=1}^N \tilde{\mathbf{A}}_i\mathbf{z}_i^{n+1} + \mathbf{m}^{n+1}) \tag{31}$$

Algorithm 1 Parallel PJ-ADMM Computing Framework for Solving CI-PASB Problem

Input: $\mathbf{s}$, $\mathbf{H}$, γ_k, P, N
Output: $\mathbf{x}^{SB*}$, q^*
1: Construct $\tilde{\mathbf{A}}$, $\tilde{\mathbf{c}}$;
2: Initialize $n=0$, $\mathbf{z}^0$, $\boldsymbol{\lambda}^0$, $\tau_i (i=1,\cdots,N)$, $\hat{\gamma}$, n_{max}, ε;
3: **repeat**
4: $n \leftarrow n+1$;
5: All processor units update $\mathbf{m}^n$ with (32);
6: **for** $i=1:N$ (parallel)
7: Processor unit i updates $\mathbf{z}_i^n$ with (34) and (35);
8: **end for**
9: Processor unit i shares $\tilde{\mathbf{A}}_i \mathbf{z}_i^n$, $\forall i \in \{1,\cdots,N\}$;
10: All processor units update $\boldsymbol{\lambda}^n$ with (31);
11: **until** $max\left\{\frac{\|\mathbf{z}^n-\mathbf{z}^{n-1}\|_2}{\|\mathbf{z}^{n-1}\|_2}, \frac{\|\boldsymbol{\lambda}^n-\boldsymbol{\lambda}^{n-1}\|_2}{\|\boldsymbol{\lambda}^{n-1}\|_2}\right\} \le \varepsilon$ *or* $n \ge n_{max}$
12: $\mathbf{z}^{opt}=\mathbf{z}^n$;
13: $\mathbf{y}^{opt}=\mathbf{G}^{-1}\mathbf{z}^{opt}$ (obtained by (22));
14: $\mathbf{x}^{SB*}=\mathbf{y}^{opt}(1:N_t)+1j\cdot\mathbf{y}^{opt}(N_t+1:2N_t)$;
15: $q^*=\mathbf{y}^{opt}(2N_t+1)$;

where we note that $\frac{1}{2}\|\mathbf{z}_i-\mathbf{z}_i^n\|_{\mathbf{P}_i}^2$ in (30) is the introduced proximal term to ensure convergence, and $\hat{\gamma}>0$ is the damping parameter. [3]

It is trivial to obtain the closed-form solution of subproblem (29) as follows

$$\mathbf{m}^{n+1}=max\left\{\tilde{\mathbf{A}}\mathbf{z}^n-\frac{\boldsymbol{\lambda}^n}{\rho},\mathbf{0}\right\}, \tag{32}$$

which is derived by setting the gradient of $\mathcal{L}_{aug}(\mathbf{z}_{i,i=1,\cdots,N}^n,\mathbf{m},\boldsymbol{\lambda}^n)$ to zero, and then projecting the critical point onto the non-negative feasible domain. As for subproblem (30), initially it appears that there is no closed-form solution due to the constraint $\mathbf{z}_i\in\chi_i$, and hence iterative algorithm for solving that may be necessary. However, in ***Proposition 2*** we will demonstrate that the optimal solution of (30) can be obtained by closed-form computations, which can significantly reduce the complexity compared with the iteration-based method.

Proposition 2: The optimal solution $\mathbf{z}_i^{opt}$ of (30) can be derived with the following two steps.

1) **Step one**: We consider an unconstrained version of (30)

$$\min f(\mathbf{z}_i), \tag{33}$$

where $f(\mathbf{z}_i)=\mathcal{L}_{aug}(\mathbf{z}_i,\mathbf{z}_{j,j\neq i}^n,\mathbf{m}^{n+1},\boldsymbol{\lambda}^n)+\frac{1}{2}\|\mathbf{z}_i-\mathbf{z}_i^n\|_{\mathbf{P}_i}^2$. Setting the gradient of $f(\mathbf{z}_i)$ to $\mathbf{0}$, we can obtain the critical point $\mathbf{z}_i^\star$ as

$$\mathbf{z}_i^\star=\mathbf{z}_i^n-\frac{1}{\tau_i}\tilde{\mathbf{c}}_i-\frac{1}{\tau_i}\rho\tilde{\mathbf{A}}_i^T(\tilde{\mathbf{A}}\mathbf{z}^n-\mathbf{m}^{n+1}-\frac{\boldsymbol{\lambda}^n}{\rho}). \tag{34}$$

[3]There are multiple ways to choose the matrix $\mathbf{P}_i$. In this paper, we adopt $\mathbf{P}_i=\tau_i\mathbf{I}-\rho\tilde{\mathbf{A}}_i^T\tilde{\mathbf{A}}_i$, which can facilitate the derivations in ***Proposition 2***, and we note that $\tau_i>0$. For other selection methods, please refer to [38].

2) **Step two**: Projecting $\mathbf{z}_i^\star$ onto χ_i, i.e.,

$$\{z_{i,l}^{opt},z_{i,l+1}^{opt}\}= \begin{cases}\{z_{i,l}^\star,z_{i,l+1}^\star\}, & if\ (z_{i,l}^\star)^2+(z_{i,l+1}^\star)^2\le P\\ \{\frac{\sqrt{P}\cdot z_{i,l}^\star}{\sqrt{(z_{i,l}^\star)^2+(z_{i,l+1}^\star)^2}},\frac{\sqrt{P}\cdot z_{i,l+1}^\star}{\sqrt{(z_{i,l}^\star)^2+(z_{i,l+1}^\star)^2}}\}, & otherwise\end{cases} \quad \forall l\in\mathcal{O} \tag{35}$$

where $\mathcal{O}=\{1,3,5,\cdots,\frac{2N_t}{N}-1\}$ and $z_{i,l}^\star$ ($z_{i,l}^{opt}$) denotes the l-th entry of $\mathbf{z}_i^\star$ ($\mathbf{z}_i^{opt}$). Then, the optimal solution $\mathbf{z}_i^{opt}$ can be obtained by combining all $\{z_{i,l}^{opt},z_{i,l+1}^{opt}\}$ into a compact vector orderly. It should be noted that, for the case of $i=N$, an additional term $z_{N,\frac{2N_t}{N}+1}^\star$ (i.e., variable q in (12)) needs to be added to the end of $\mathbf{z}_N^{opt}$ as q is independent of the constraint $\mathbf{z}_i\in\chi_i$.

Proof:See Appendix.

Based on the descriptions presented above, we propose an overall parallel computing framework, as shown in **Algorithm 1**. This framework employs N processor units for parallel computation and facilitates inter-unit communication via dedicated fully connected links. We note that the i-th unit stores $\tilde{\mathbf{A}}_i$ instead of the full $\tilde{\mathbf{A}}$ in order to reduce memory usage. During the sharing phase, for the i-th unit, we can share the product $\tilde{\mathbf{A}}_i\mathbf{z}_i$ instead of $\{\tilde{\mathbf{A}}_i,\mathbf{z}_i\}$ to decrease the communication overhead.

D. Convergence Analysis

In this subsection, we discuss the convergence of the proposed parallel algorithm. It is noted that problem (26) shares the same form as the problem discussed in [38], with the addition of an auxiliary variable $\mathbf{m}$. However, according to the conclusions in [22], such an auxiliary variable does not affect the convergence of the parallel PJ-ADMM algorithm. Therefore, the convergence proof in [38] can be directly applied to our proposed algorithm. Specifically, for $n\ge 1$, we have

$$\left\|\mathbf{u}^n-\mathbf{u}^{opt}\right\|_{\mathbf{Q}}^2-\left\|\mathbf{u}^{n+1}-\mathbf{u}^{opt}\right\|_{\mathbf{Q}}^2\ge\eta\cdot\left\|\mathbf{u}^n-\mathbf{u}^{n+1}\right\|^2, \tag{36}$$

where $\mathbf{u}^n=[(\mathbf{z}_1^n)^T,\cdots,(\mathbf{z}_N^n)^T,(\boldsymbol{\lambda}^n)^T]^T$, and $\mathbf{u}^{opt}=[(\mathbf{z}^{opt})^T,(\boldsymbol{\lambda}^{opt})^T]^T$ represents the optimal solution that the algorithm will eventually converge to. Moreover, η is a positive number, and $\mathbf{Q}$ has the following structure

$$\mathbf{Q}=\begin{bmatrix}\tau_1\mathbf{I} & & & \\ & \ddots & & \\ & & \tau_N\mathbf{I} & \\ & & & \frac{1}{\hat{\gamma}\rho}\mathbf{I}\end{bmatrix}. \tag{37}$$

From (36), it can be seen that since $\left\|\mathbf{u}^n-\mathbf{u}^{n+1}\right\|^2\ge 0$, the iterative sequence $\{\mathbf{u}^n\}$ is strictly contractive, which indicates that **Algorithm 1** can converge to the optimal solution. Furthermore, we can establish the $O(1/n)$ convergence rate for **Algorithm 1**. More details on the proof of (36) and the convergence rate can be found in [38], which is omitted in this paper for brevity.

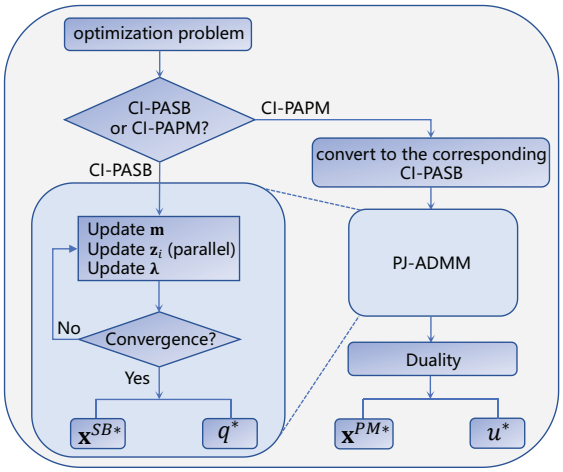

Fig. 2: Flowchart for Parallel Solution.

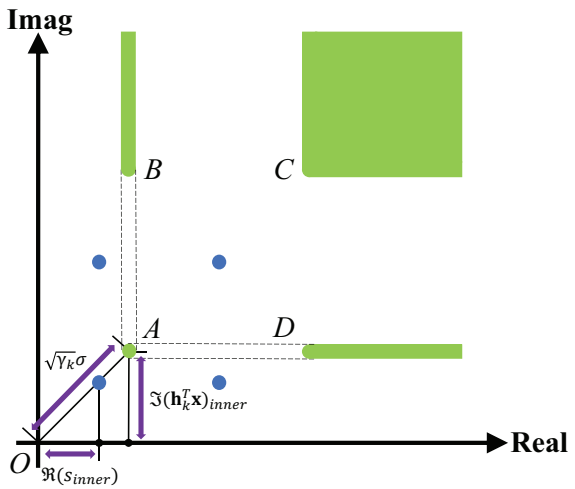

Fig. 3: Symbol scaling metric for QAM signaling, 16QAM. [4]

E. Parallel Solution for CI-PAPM Problem

According to the duality relation presented in (14), we can obtain the optimal solution to the CI-PAPM problem based on the solution to the CI-PASB problem. Therefore, given the motivation for parallel processing and the unseparable nature of (10), the parallel framework outlined in the previous subsection can be seamlessly applied to tackle the CI-PAPM problem. To be more specific, given the input $(\mathbf{b}, P)$, we can first address the corresponding CI-PASB problem with **Algorithm 1** and obtain the optimal solution $\{q^*, \mathbf{x}^{SB*}\}$. Subsequently, the optimal solution $\{u^*, \mathbf{x}^{PM*}\}$ of the CI-PAPM problem can be obtained as

$$u^* = \frac{P}{(q^*)^2}, \quad \mathbf{x}^{PM*} = \frac{\Re(\mathbf{x}^{SB*})}{q^*} + 1j \cdot \frac{\Im(\mathbf{x}^{SB*})}{q^*}, \tag{38}$$

where it is worth noting that the selection of power boundary P does not affect the optimal solution (38), and for convenience we can set $P = 1/N_t$.

Finally, as a summary of this Section, we provide the flowchart for the parallel solution to the CI-PASB problem and the CI-PAPM problem, as shown in Fig. 2.

IV. Parallel Solutions for CI-PASB Problem and CI-PAPM Problem with QAM Signaling

In this section, we extend the parallel solutions in the previous section to QAM signaling. Firstly, we will introduce the symbol scaling metric of CI precoding and construct the CI-PASB problem and the CI-PAPM problem under QAM, along with the proof of the duality between them. Subsequently, by making a minor adjustment to the PJ-ADMM framework introduced in the previous section, it can be effectively employed to address the separable CI-PASB problem under QAM. As for the unseparable CI-PAPM problem, by referring to the previous section, we can use the established duality to transform its solution to the solution of its CI-PASB counterpart.

A. Symbol Scaling Metric and Problem Formulations

In contrast to the CI precoding under PSK, CI precoding design under QAM allows for interference exploitation only at the outer constellation points. As shown in Fig. 3, the real and imaginary parts of point C, the imaginary part of point B, and the real part of point D can be utilized for CI, but due to the detection threshold limitations, the real and imaginary parts of point A, the real part of point B, and the imaginary part of point D cannot be used for interference exploitation. Symbol scaling metric can be employed to describe the above characteristic. Specifically, for user k, we decompose the received noiseless constellation point $\mathbf{h}_k^T\mathbf{x}$ along the real and imaginary axes, and then introduce a scaling factor α_s to express the received signal as

$$\Re(\mathbf{h}_k^T\mathbf{x}) \trianglerighteq \alpha_s \cdot \Re(s_k), \quad \Im(\mathbf{h}_k^T\mathbf{x}) \trianglerighteq \alpha_s \cdot \Im(s_k), \tag{39}$$

where the notation $\trianglerighteq$ represents $\geq$ or $=$, which depends on whether the real and imaginary parts of s_k can be exploited. Regarding the expression of α_s, we can illustrate it using the innermost normalized constellation point s_{inner} located in the first quadrant (for 16-QAM, $s_{inner} = \frac{1}{\sqrt{10}} + j \cdot \frac{1}{\sqrt{10}}$), where under that case (39) can be rewritten as

$$\Re(\mathbf{h}_k^T\mathbf{x})_{inner} = \alpha_s \cdot \Re(s_{inner}), \Im(\mathbf{h}_k^T\mathbf{x})_{inner} = \alpha_s \cdot \Im(s_{inner}). \tag{40}$$

In Fig. 3, given the SINR boundary γ_k and the fact that point A owns the minimum SINR among all received constellation points, we can directly obtain that $\alpha_s = \frac{\sqrt{\gamma_k}\sigma}{\sqrt{2}\cdot\Re(s_{inner})}$. Then, expanding the above analysis from the first quadrant to all quadrants, we can derive the CI conditions for user k corresponding to the symbol scaling metric as below

$$sign(\Re(s_k)) \cdot \Re(\mathbf{h}_k^T\mathbf{x}) \trianglerighteq sign(\Re(s_k)) \cdot \frac{\sqrt{\gamma_k}\sigma}{\sqrt{2} \cdot \Re(s_{inner})} \cdot \Re(s_k), \tag{41}$$

[4]The blue dots represent the normalized 16QAM constellation points located in the first quadrant, while the green area (CI region) is composed of the received constellation points.

$$sign(\Im(s_k))\cdot\Im(\mathbf{h}_k^T\mathbf{x}) \trianglerighteq sign(\Im(s_k))\cdot\frac{\sqrt{\gamma_k}\sigma}{\sqrt{2}\cdot\Im(s_{inner})}\cdot\Im(s_k), \tag{42}$$

Letting $\hat{\mathbf{h}}_k^T = \frac{\mathbf{h}_k^T}{\Re(s_k)}$ and $\bar{\mathbf{h}}_k^T = \frac{\mathbf{h}_k^T}{\Im(s_k)}$, (41) and (42) can be simplified as

$$\Re(\hat{\mathbf{h}}_k^T\mathbf{x}) \trianglerighteq \frac{\sqrt{\gamma_k}\sigma}{\sqrt{2}\cdot\Re(s_{inner})}, \tag{43}$$

$$\Im(\bar{\mathbf{h}}_k^T\mathbf{x}) \trianglerighteq \frac{\sqrt{\gamma_k}\sigma}{\sqrt{2}\cdot\Im(s_{inner})}. \tag{44}$$

Furthermore, by introducing $\hat{\mathbf{x}} = \begin{bmatrix}\Re(\mathbf{x})\\ \Im(\mathbf{x})\end{bmatrix}$, $\hat{\mathbf{S}}_k = \begin{bmatrix}\frac{1}{\Re(s_k)} & 0\\ 0 & \frac{1}{\Im(s_k)}\end{bmatrix}$, $\mathbf{H}_k = \begin{bmatrix}\Re(\mathbf{h}_k^T) & -\Im(\mathbf{h}_k^T)\\ \Im(\mathbf{h}_k^T) & \Re(\mathbf{h}_k^T)\end{bmatrix}$, $\mathbf{A}_k = \hat{\mathbf{S}}_k\mathbf{H}_k$, $\mathbf{b}_k = \frac{\sqrt{\gamma_k}\sigma}{\sqrt{2}\cdot\Re(s_{inner})}\cdot\mathbf{1}$, $\mathbf{A} = [\mathbf{A}_1^T,\cdots,\mathbf{A}_K^T]^T$ and $\mathbf{b} = [\mathbf{b}_1^T,\cdots,\mathbf{b}_K^T]^T$, we can obtain the real-value equivalence of (43) and (44) as

$$\mathbf{A}\hat{\mathbf{x}} \trianglerighteq \mathbf{b}, \tag{45}$$

where in order to derive the problem formulations similar to that under PSK modulation, we abuse the notations $\mathbf{A}$ and $\mathbf{b}$.

With the constraints (45), the CI-PAPM problem under QAM can be expressed as

$$\begin{aligned}&\min_{\hat{\mathbf{x}},u}\ u\\ &s.t.\mathbf{A}\hat{\mathbf{x}} \trianglerighteq \mathbf{b}\\ &\quad\hat{\mathbf{x}}^T\mathbf{E}_j\hat{\mathbf{x}} \le u,\ \forall j\in\{1,\cdots,N_t\},\end{aligned} \tag{46}$$

and the corresponding CI-PASB problem is

$$\begin{aligned}&\max_{\hat{\mathbf{x}},q}\ q\\ &s.t.\mathbf{A}\hat{\mathbf{x}} \trianglerighteq q\cdot\mathbf{b}\\ &\quad\hat{\mathbf{x}}^T\mathbf{E}_j\hat{\mathbf{x}} \le P,\ \forall j\in\{1,\cdots,N_t\}.\end{aligned} \tag{47}$$

As can be observed, formulations (46) and (47) are similar to those under PSK modulation, with the only difference being that the notation used in the CI conditions is $\trianglerighteq$ instead of $\succeq$.

B. Duality Between CI-PASB and CI-PAPM under QAM

Proposition 3: The duality built in ***Proposition 1*** still holds true for problem (46) and problem (47).

Proof: By substituting $\trianglerighteq$ for $\succeq$ in the proof process of ***Proposition 1***, with all other steps unchanged, we can directly conclude that duality holds under QAM modulation. ■

C. Parallel Solution for CI-PASB Problem

Considering that problem (12) and problem (47) share the same formulation except for the notation $\trianglerighteq$, we can directly write the separable version of (47) as

$$\begin{aligned}&\min_{\mathbf{z}_i\in\chi_i}\ \sum_{i=1}^{N}\tilde{\mathbf{c}}_i^T\mathbf{z}_i\\ &s.t.\ \sum_{i=1}^{N}\tilde{\mathbf{A}}_i\mathbf{z}_i \trianglerighteq \mathbf{0},\end{aligned} \tag{48}$$

where the construction of $\tilde{\mathbf{c}}_i$, $\mathbf{z}_i$, $\tilde{\mathbf{A}}_i$ and χ_i is the same as that in the previous section. To facilitate the following derivations, (48) can be further rewritten as below

$$\begin{aligned}&\min_{\mathbf{m},\ \mathbf{z}_i\in\chi_i}\ \sum_{i=1}^{N}\tilde{\mathbf{c}}_i^T\mathbf{z}_i + \hat{I}(\mathbf{m})\\ &s.t.\ \mathbf{m} = \sum_{i=1}^{N}\tilde{\mathbf{A}}_i\mathbf{z}_i,\end{aligned} \tag{49}$$

where $\mathbf{m}$ is the introduced auxiliary variable, and $\hat{I}(\mathbf{m})$ is the indicator function given by

$$\hat{I}(\mathbf{m}) = \begin{cases}0, & if\ \mathbf{m}\in M^{QAM}\\ \infty, & otherwise\end{cases} \tag{50}$$

We note that, M^{QAM} in (50) represents the set $M^{QAM} = \{\mathbf{m}\mid m_i\ge 0, i\in S^{QAM}; m_i = 0, i\notin S^{QAM}\}$, and S^{QAM} denotes the index set that contains the indices of the real or imaginary parts of the constellation points that can be used for interference exploitation.

In the following, we will demonstrate the specific steps of solving (49) using the PJ-ADMM algorithm. Firstly, with the penalty parameter ρ and the Lagrangian multiplier $\boldsymbol{\lambda}$, the augmented Lagrangian of (49) can be derived as

$$\begin{aligned}\mathcal{L}_{aug} =& \sum_{i=1}^{N}\tilde{\mathbf{c}}_i^T\mathbf{z}_i + \hat{I}(\mathbf{m})\\ &+\boldsymbol{\lambda}^T\cdot(\mathbf{m}-\sum_{i=1}^{N}\tilde{\mathbf{A}}_i\mathbf{z}_i) + \frac{\rho}{2}\Big\|\mathbf{m}-\sum_{i=1}^{N}\tilde{\mathbf{A}}_i\mathbf{z}_i\Big\|_2^2.\end{aligned} \tag{51}$$

According to the PJ-ADMM algorithm, each PJ-ADMM iteration involves the updates of variables $\mathbf{m}$, $\mathbf{z}_i$, and $\boldsymbol{\lambda}$. Thereinto, it is worth noting that the updates of $\mathbf{z}_i$ and $\boldsymbol{\lambda}$ remain unchanged compared with that under PSK modulation, while the only difference is the update of $\mathbf{m}$. Specifically, we can update $\mathbf{m}$ as follows

$$m_i = \begin{cases}max\{[\tilde{\mathbf{A}}\mathbf{z}^n - \frac{\boldsymbol{\lambda}^n}{\rho}]_i, 0\}, & if\ i\in S^{QAM}\\ 0, & otherwise\end{cases} \tag{52}$$

where $\mathbf{m} = [m_1,\cdots,m_{2K}]^T$, and $[\tilde{\mathbf{A}}\mathbf{z}^n - \frac{\boldsymbol{\lambda}^n}{\rho}]_i$ denotes the i-th entry of vector $\tilde{\mathbf{A}}\mathbf{z}^n - \frac{\boldsymbol{\lambda}^n}{\rho}$. Subsequently, by replacing the update equation (32) for variable $\mathbf{m}$ with equation (52), we can directly utilize the parallel PJ-ADMM framework presented in **Algorithm 1** to solve the CI-PASB problem under QAM.

D. Parallel Solution for CI-PAPM Problem

Similar to the case under PSK modulation, the CI-PAPM problem under QAM is also unseparable such that the existing parallel method cannot be directly used. However, with the established duality presented in ***Proposition 3***, we can transform the solution of (46) into solving its CI-PASB counterpart (47), and hence both of these two problems under QAM can be tackled in the same parallel framework.

TABLE I
NUMBER OF MULTIPLICATIONS AND ADDITIONS REQUIRED IN EACH ITERATION

Updates	Multiplications	Additions
$\mathbf{m}$	$(2K+2)N$	$2KN$
$\mathbf{z}$	$(2N_t+1)(2K+1)$ $+2KN+25N_t+2N$	$(4N_t+2)K+2KN$ $+11N_t+1$
$\boldsymbol{\lambda}$	$(4N_t+4N+2)K+N$	$(2N^2+4N_t+2)K$

V. COMPLEXITY ANALYSIS

In this section, taking phase rotation metric as an example, we will evaluate the complexity of **Algorithm 1** by analyzing the communication overhead and the total number of required floating-point operations [41].

Given a parallel framework with N processor units, for the i-th unit, the dimension of the shared vector $\tilde{\mathbf{A}}_i\mathbf{z}_i$ is $2K \times 1$ in each communication procedure. Therefore, the overall communication overhead can be expressed as $2KN(N-1)I_{ite}\kappa$, where I_{ite} is the average number of iterations, and κ represents the number of bits required to exchange a single real-valued scalar [22].

Regarding the number of floating-point operations, we have provided a detailed breakdown in TABLE I, taking into account all floating-point operations on N processors. Then, by summing up the expressions in TABLE I, we can obtain the total number of multiplications and additions as U_m and U_a, respectively. As can be observed, the overall computational complexity is on the order of $\mathbb{O}(KN^2+KN_t)$ in each iteration. When employing the primal-dual interior point method (IPM) to solve (9) and (11), its complexity upper bound is $\mathbb{O}(N_t^{3.5}log(N_t/\epsilon_{tol}))$, where ϵ_{tol} denotes the optimality tolerance. Hence, theoretically, the proposed parallel method exhibits superior complexity compared to IPM.

$$U_m = (8KN+8KN_t+27N_t+5N+4K+1)\cdot I_{ite} \quad (53)$$

$$U_a = (2KN^2+4KN+8KN_t+11N_t+4K+1)\cdot I_{ite} \quad (54)$$

VI. NUMERICAL RESULTS

We employ Monte Carlo methods to verify our proposed parallel algorithm. In the simulation results, Rayleigh flat-fading channel $\mathbf{H}$ with entries that follow the standard complex Gaussian distribution is used. In the simulations of symbol error rate (SER) performance, for convenience, we assume that the total transmit power is 1 and the per-antenna power constraint thus becomes $P = \frac{1}{N_t}$. We note that when the proposed algorithm is applied to practical systems, the per-antenna power limit P can be easily adjusted to the parameter required by the actual system. Moreover, it should be noted that the built-in 'parfor' tool in MATLAB cannot be used to validate the proposed parallel algorithm due to significant communication overhead. Considering that our study focuses on the mechanism of the parallel algorithm rather than its specific hardware implementation, we implement this parallel algorithm in a serial manner for the simulations in this section.

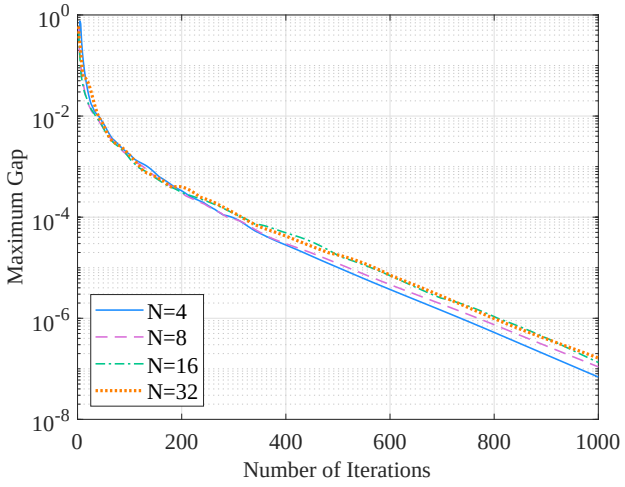

Fig. 4: Maximum gap v.s. number of iterations, $N_t = 64$, $K = 32$, $N = \{4, 8, 16, 32\}$, QPSK.

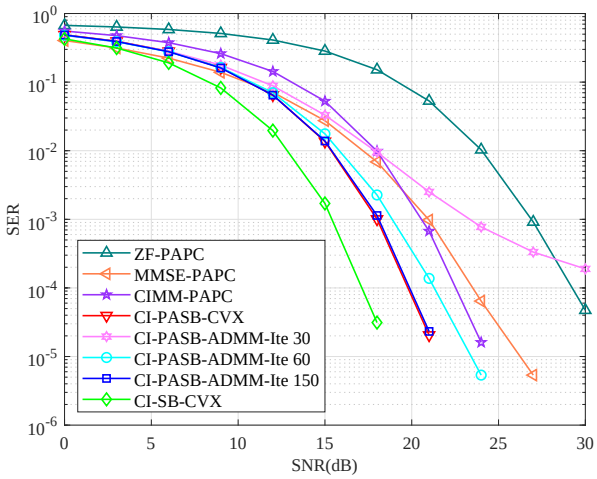

Fig. 5: SER v.s. SNR, $n_{max} = \{30, 60, 150\}$, $N_t = 64$, $K = 56$, $N = 16$, QPSK.

Specifically, in each iteration, the variable $\mathbf{z}$ is updated sequentially by first updating $\mathbf{z}_1$, then $\mathbf{z}_2$, and so on, in the specified order. The initialization parameters in PJ-ADMM iterations are $\mathbf{z}^0 = [\mathbf{0}^T, q_0]^T$, $q_0 = 5$, $\boldsymbol{\lambda}^0 = \mathbf{0}$, $\tau_i = \alpha_\tau \frac{\rho N}{2-\hat{\gamma}} \left\|\tilde{\mathbf{A}}_i\right\|_F^2$, $\alpha_\tau = 0.1$.[5] For the problem under PSK modulation, the values of ρ and $\hat{\gamma}$ are set as $\rho = 0.01, \hat{\gamma} = 0.1$, while for the problem under QAM modulation, the values are set as $\rho = 0.001, \hat{\gamma} = 0.5$. Moreover, in order to make the parallel algorithm proposed in this paper easily applicable to other scenarios, we provide the reference ranges for some important parameters in the PJ-ADMM algorithm, which are $q_0 \geq 0$, $0.05 \leq \alpha_\tau \leq 0.5$, $0.001 \leq \rho \leq 0.1$, $0.01 \leq \hat{\gamma} \leq 0.5$.

[5]According to the convergence analysis in [38], when $\mathbf{P}_i = \tau_i\mathbf{I} - \rho\tilde{\mathbf{A}}_i^T\tilde{\mathbf{A}}_i$ the initial τ_i requires to satisfy $\tau_i > \frac{\rho N}{2-\hat{\gamma}} \left\|\tilde{\mathbf{A}}_i\right\|_2^2$. However, due to the much higher complexity of computing $\left\|\tilde{\mathbf{A}}_i\right\|_2^2$, we substitute $\left\|\tilde{\mathbf{A}}_i\right\|_F^2$ for $\left\|\tilde{\mathbf{A}}_i\right\|_2^2$ and further introduce the scaling parameter α_τ to guarantee the convergence, and hence we set $\tau_i = \alpha_\tau \frac{\rho N}{2-\hat{\gamma}} \left\|\tilde{\mathbf{A}}_i\right\|_F^2$.

This article has been accepted for publication in IEEE Transactions on Communications. This is the author's version which has not been fully edited and content may change prior to final publication. Citation information: DOI 10.1109/TCOMM.2025.3541106

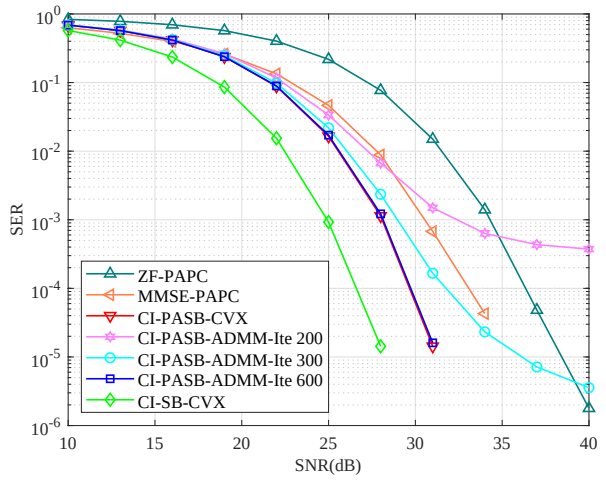

Fig. 6: SER v.s. SNR, $n_{max} = \{200, 300, 600\}$, $N_t = 64$, $K = 56$, $N = 16$, 16QAM.

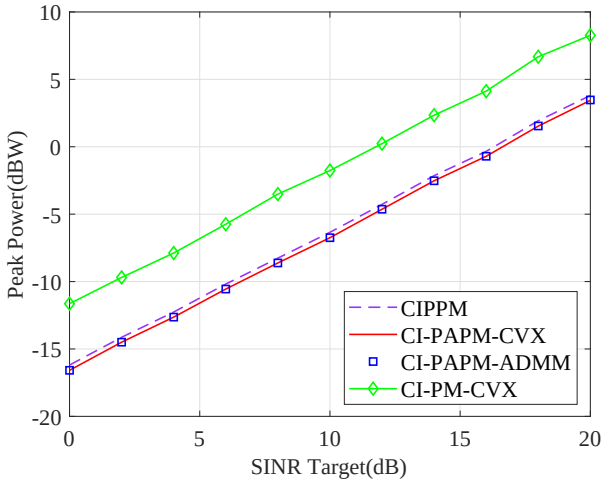

Fig. 8: Peak power v.s. SINR target, $N_t = 64$, $K = 32$, $N = 16$, QPSK.

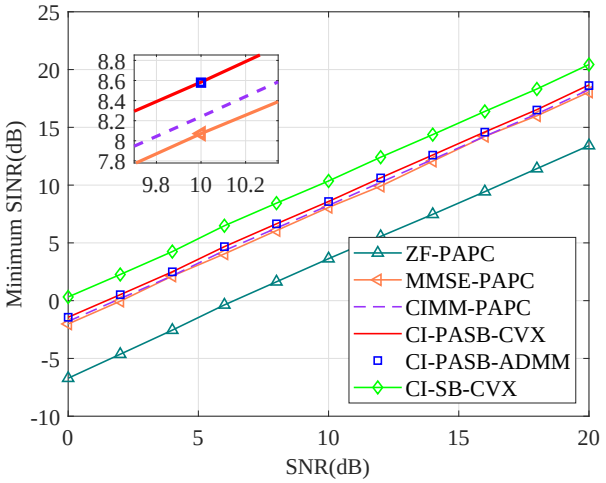

Fig. 7: Minimum SINR v.s. SNR, $N_t = 64$, $K = 32$, $N = 16$, QPSK.

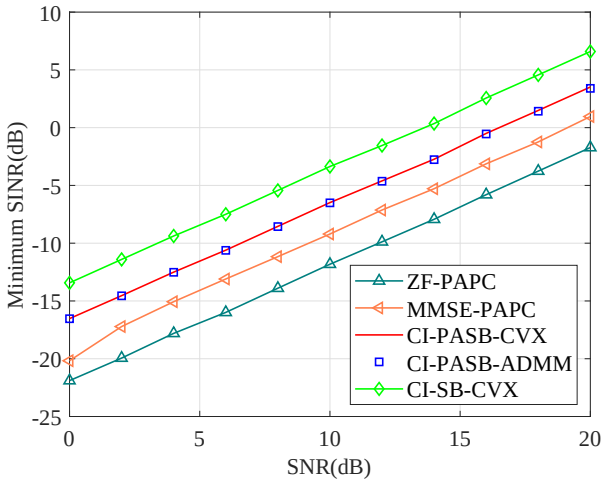

Fig. 9: Minimum SINR v.s. SNR, $N_t = 64$, $K = 56$, $N = 16$, 16QAM.

For clarity, the abbreviations we use in our simulation results are presented as below:

1) 'ZF-PAPC': zero-forcing precoder that satisfies per-antenna power constraint, whose precoding structure is $\mathbf{W}_{\mathrm{ZF-PAPC}} = \sqrt{P} \cdot \beta_{\mathrm{ZF-PAPC}} \cdot \mathbf{H}^{\dagger}$, where $\beta_{\mathrm{ZF-PAPC}} = 1/(\max_i \left|\left[\mathbf{H}^{\dagger}\mathbf{s}\right]_i\right|)$.
2) 'MMSE-PAPC': minimum mean squared error precoder with per-antenna power constraint [42].
3) 'CIPPM': constructive interference for peak power minimization problem with strict phase rotation metric [33].
4) 'CIMM-PAPC': constructive interference max-min fair problem with per-antenna power constraint, where the strict phase rotation metric is employed [34].
5) 'CI-PAPM-CVX(or ADMM)': CI-PAPM problem solved by optimization tools CVX (or our proposed parallel ADMM method).
6) 'CI-PASB-CVX(or ADMM)': CI-PASB problem solved by optimization tools CVX (or our proposed parallel ADMM method).
7) 'CI-PM(or SB)-CVX': constructive interference sum power minimization problem with SINR constraints [19] (or constructive interference SINR balancing problem with sum-power constraint [23]) solved by optimization tools CVX.
8) 'CI-PASB-PG(or CF)': CI-PASB problem with PSK signaling solved by the projected gradient framework [36] (or the closed-form solution based method [37]).

In Fig. 4, we demonstrate the convergence behavior of the proposed parallel ADMM approach, where $\varepsilon = 10^{-8}$, $n_{max} = 1000$, and $max\left\{\frac{\|\mathbf{z}^{n+1}-\mathbf{z}^{n}\|_2}{\|\mathbf{z}^{n}\|_2}, \frac{\|\boldsymbol{\lambda}^{n+1}-\boldsymbol{\lambda}^{n}\|_2}{\|\boldsymbol{\lambda}^{n}\|_2}\right\}$ denotes the maximum gap. It can be observed that the PJ-ADMM method converges for various values of N, with an initially fast convergence rate that gradually slows down.

Fig. 5 shows the SER performance of different SINR balancing based precoders, where $\varepsilon = 10^{-5}$, and $n_{max} =$

This article has been accepted for publication in IEEE Transactions on Communications. This is the author's version which has not been fully edited and content may change prior to final publication. Citation information: DOI 10.1109/TCOMM.2025.3541106

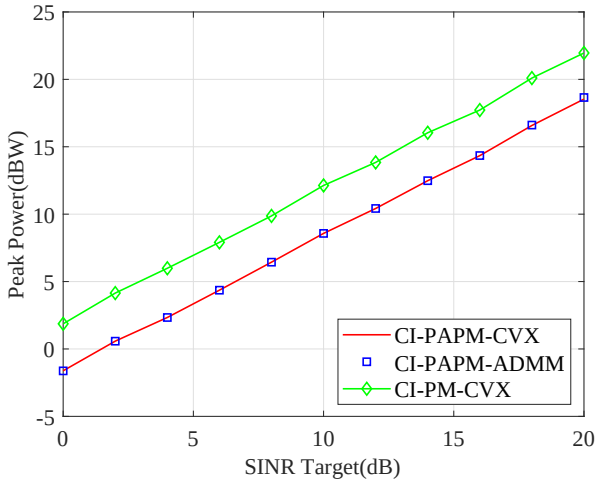

Fig. 10: Peak power v.s. SINR target, $N_t = 64$, $K = 56$, $N = 16$, 16QAM.

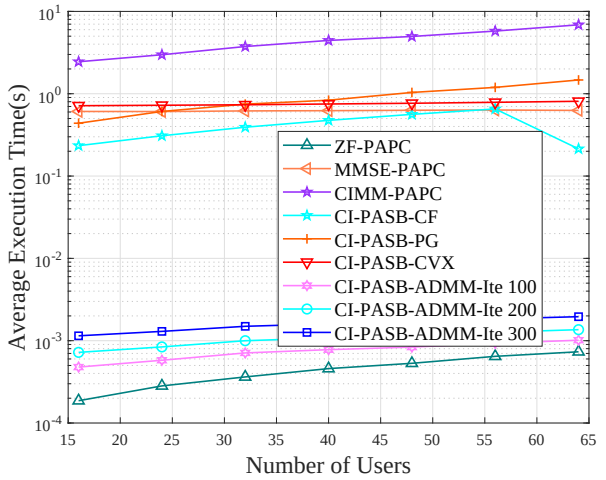

Fig. 11: Average execution time v.s. number of users, $n_{max} = \{100, 200, 300\}$, $N_t = 64$, $K = 16 : 8 : 64$, $N = 16$, QPSK.

$\{30, 60, 150\}$. The SNR refers to the signal-to-noise ratio at the transmitter, which is expressed as $\frac{P_{sum}}{\sigma^2}$, where P_{sum} represents the total transmit power and σ^2 is the noise power. Due to the inherent inability to utilize interference and the significant reduction in energy efficiency caused by the scaling parameter $\sqrt{P} \cdot \beta_{\mathrm{ZF-PAPC}}$, the ZF-PAPC precoder demonstrates the worst SER performance. Moreover, since the usage of strict phase rotation metric, the performance of 'CIMM-PAPC' is poor than 'CI-PASB-CVX' that uses more advanced non-strict phase rotation metric. On the other hand, with the iteration number n_{max} increasing, the SER performance of parallel ADMM method gradually approaches optimality, which verifies the effectiveness of our proposed algorithm. In Fig. 6, we extend the SER simulation to 16QAM scenarios. It is observed that our proposed method remains effective, although a higher number of iterations is required to achieve optimality. This is because the minimum distance between constellation points in 16QAM is smaller than in QPSK, requiring a smaller threshold ε and more iterations. Moreover, in both Fig. 5 and Fig. 6, the 'CI-PASB-ADMM' scheme exhibits error floor with 30 iterations of ADMM, which occurs because 'CI-PASB-ADMM' has not yet converged to the optimal solution at the corresponding number of iterations. It should be mentioned that, if we continue to increase n_{max}, the ADMM algorithm will reach optimality finally, but the performance improvement achieved by excessive iterations may not be significant.

Fig. 7 shows the relation between the achieved minimum SINR and the SNR of various SINR balancing based precoders. We set the per-antenna power constraint as $P = \frac{P_{sum}}{N_t}$ and the noise power as $\sigma^2 = 1$. Firstly, our proposed 'CI-PASB-ADMM' can obtain the same minimum SINR as that in the 'CI-PASB-CVX' method. Then, we can observe that the performance of 'CIMM-PAPC' is worse than 'CI-PASB-CVX' due to the suboptimal strict phase rotation metric used in 'CIMM-PAPC'. We also note that, since the per-antenna power constraint is more restrictive than the total power constraint, 'CI-SB-CVX' method can achieve better SINR performance compared with 'CI-PASB-ADMM' method.

Fig. 8 shows the achieved peak power of various power minimization based methods. First of all, both 'CI-PAPM-ADMM' and 'CI-PAPM-CVX' obtain the same peak power performance, which verifies the parallel method and the established duality. Most importantly, from Fig. 8 we can obtain that the peak power of 'CI-PM-CVX' is decreased when per-antenna power constraint is considered, which means that our proposed 'CI-PAPM-ADMM' method can effectively reduce the peak power and further improve the system performance.

In Fig. 9 and Fig. 10, we extend the simulations from Fig. 7 and Fig. 8, respectively, to consider precoding design under QAM modulation. We highlight that the parallel method and the established duality proposed in Section IV remain effective.

In Fig. 11, we present the average execution time of different SINR balancing based precoders. It is worth noting that the parallel ADMM method exhibits much lower complexity compared to the centralized methods 'CI-PASB-CF', 'CI-PASB-PG' and 'CI-PASB-CVX'. Moreover, within a fewer number of iterations, the complexity of the parallel method approaches that of 'ZF-PAPC'. For the curve of 'CI-PASB-CF', there is a strange decrease when $K = 64$, where the specific reason is that under $K = N_t$, the closed-form precoder structure can be simplified, leading to a reduction in the dimension of the optimization variable. Furthermore,

TABLE II
NUMBER OF FLOATING-POINT OPERATIONS REQUIRED IN EACH ITERATION, $N_t = 64$, QPSK.

	$K = 16$	$K = 32$	$K = 48$	$K = 64$
$N = 4$	2.02×10^4	3.8×10^4	5.58×10^4	7.36×10^4
$N = 8$	2.26×10^4	4.27×10^4	6.28×10^4	8.29×10^4
$N = 16$	3.03×10^4	5.81×10^4	8.58×10^4	1.14×10^5
$N = 32$	5.8×10^4	1.13×10^5	1.69×10^5	2.24×10^5

in TABLE II we provide the total number of floating-point operations required in each PJ-ADMM iteration, showing an approximate linear growth with increasing K. While the total floating-point operations are of the order $\mathbb{O}(KN^2+KN_t)$, in this TABLE they do not increase quadratically with respect to N, as this quadratic relationship only appears when N reaches very large values.

VII. Conclusion

In this paper, we investigate the parallel solution of CI precoding, with the aim of reducing computational complexity in practical PAPC scenarios. Specifically, we focus on the solution of two CI-based problems, namely, the CI-PASB problem and the CI-PAPM problem. For the separable CI-PASB problem, we propose the utilization of the PJ-ADMM algorithm as a suitable solution. For the unseparable CI-PAPM problem, we establish the duality between the two problems and leverage it to transform the solution of CI-PAPM into the solution of the related CI-PASB problem. The effectiveness of our proposed methods is confirmed through numerical results, showcasing their ability to effectively reduce complexity and achieve optimal performance. These findings serve to promote the implementation of CI precoding under PAPC scenarios.

Appendix

Proof of Proposition 2

Proof: Firstly, defining $\mathbf{d}_i=\sum_{j\neq i}\tilde{\mathbf{A}}_j\mathbf{z}_j^n-\mathbf{m}^{n+1}-\frac{\boldsymbol{\lambda}^n}{\rho}$, $\hat{\mathbf{d}}_i^T=\tilde{\mathbf{c}}_i^T+\rho\mathbf{d}_i^T\tilde{\mathbf{A}}_i-(\mathbf{z}_i^n)^T\mathbf{P}_i$ and $\tilde{d}_i=\frac{\rho}{2}\mathbf{d}_i^T\mathbf{d}_i+\frac{1}{2}(\mathbf{z}_i^n)^T\mathbf{P}_i\mathbf{z}_i^n$, we can simplify the expression of $f(\mathbf{z}_i)$ as

$$f(\mathbf{z}_i)=\mathbf{z}_i^T(\frac{1}{2}\tau_i\mathbf{I})\mathbf{z}_i+\hat{\mathbf{d}}_i^T\mathbf{z}_i+\tilde{d}_i. \tag{55}$$

Then, letting $f(\mathbf{z}_{i,j})=\mathbf{z}_{i,j}^T(\frac{1}{2}\tau_i\mathbf{I})\mathbf{z}_{i,j}+\hat{\mathbf{d}}_{i,j}^T\mathbf{z}_{i,j}$, $\mathbf{z}_i=[\mathbf{z}_{i,1}^T,\cdots,\mathbf{z}_{i,N_t/N}^T]^T$, $\hat{\mathbf{d}}_i=[\hat{\mathbf{d}}_{i,1}^T,\cdots,\hat{\mathbf{d}}_{i,N_t/N}^T]^T$ and

$$\mathbf{z}_{i,j}=\begin{cases}[z_{i,2j-1},\ z_{i,2j},\ z_{i,2j+1}]^T & i=N, j=N_t/N\\ [z_{i,2j-1},\ z_{i,2j}]^T & otherwise\end{cases}$$

(55) can be further simplified as

$$f(\mathbf{z}_i)=\sum_{j=1}^{\frac{N_t}{N}}[\mathbf{z}_{i,j}^T(\frac{1}{2}\tau_i\mathbf{I})\mathbf{z}_{i,j}+\hat{\mathbf{d}}_{i,j}^T\mathbf{z}_{i,j}]+\tilde{d}_i=\sum_{j=1}^{\frac{N_t}{N}}f(\mathbf{z}_{i,j})+\tilde{d}_i. \tag{56}$$

According to (56) and the constraint set $\hat{\chi}_{i,j}=\left\{\mathbf{z}_{i,j}\mid z_{i,2j-1}^2+z_{i,2j}^2\leq P\right\}$, we can establish the equivalence relation as $\min\limits_{\mathbf{z}_i\in\chi_i}f(\mathbf{z}_i)\equiv\sum_{j=1}^{\frac{N_t}{N}}\left(\min\limits_{\mathbf{z}_{i,j}\in\hat{\chi}_{i,j}}f(\mathbf{z}_{i,j})\right)$, which indicates that when each subproblem $\min\limits_{\mathbf{z}_{i,j}\in\hat{\chi}_{i,j}}f(\mathbf{z}_{i,j})$ is optimized to its fullest potential, the original problem $\min\limits_{\mathbf{z}_i\in\chi_i}f(\mathbf{z}_i)$ will also be optimized and reach its optimal solution. Specifically, the optimal solution $\mathbf{z}_{i,j}^{opt}$ of each subproblem can be obtained independently, and finally $\mathbf{z}_i^{opt}$ can be formulated as $\mathbf{z}_i^{opt}=[(\mathbf{z}_{i,1}^{opt})^T,\cdots,(\mathbf{z}_{i,N_t/N}^{opt})^T]^T$.

Next, the KKT conditions are leveraged to derive the closed-form solution of $\min\limits_{\mathbf{z}_{i,j}\in\hat{\chi}_{i,j}}f(\mathbf{z}_{i,j})$. To further elaborate, we choose $\mathbf{z}_{i,j}=[z_{i,2j-1},\ z_{i,2j}]^T$ as an example and write $f(\mathbf{z}_{i,j})$ as below

$$f(\mathbf{z}_{i,j})=\frac{\tau_i}{2}z_{i,2j-1}^2+\frac{\tau_i}{2}z_{i,2j}^2+\hat{d}_{i,2j-1}\cdot z_{i,2j-1}+\hat{d}_{i,2j}\cdot z_{i,2j}. \tag{57}$$

For clarity, letting $a=\frac{\tau_i}{2}$, $z_{i,2j-1}=g_1$, $z_{i,2j}=g_2$, $\hat{d}_{i,2j-1}=v_1$ and $\hat{d}_{i,2j}=v_2$, we can transform $\min\limits_{\mathbf{z}_{i,j}\in\hat{\chi}_{i,j}}f(\mathbf{z}_{i,j})$ into its equivalent problem, which is given by

$$\begin{aligned}&\min_{g_1,g_2}\ I(g_1,g_2)=ag_1^2+ag_2^2+v_1g_1+v_2g_2\\ &s.t.\ g_1^2+g_2^2\leq P.\end{aligned} \tag{58}$$

To proceed with (58), by using the Lagrangian multiplier λ, we can construct the Lagrangian function as

$$\mathcal{L}=ag_1^2+ag_2^2+v_1g_1+v_2g_2+\lambda\cdot(g_1^2+g_2^2-P), \tag{59}$$

and the KKT conditions as

$$g_1^2+g_2^2\leq P \tag{60a}$$
$$\lambda\geq 0 \tag{60b}$$
$$\frac{\partial I(g_1,g_2)}{\partial g_1}=(2a+2\lambda)g_1+v_1=0 \tag{60c}$$
$$\frac{\partial I(g_1,g_2)}{\partial g_2}=(2a+2\lambda)g_2+v_2=0 \tag{60d}$$
$$\lambda(g_1^2+g_2^2-P)=0 \tag{60e}$$

Considering the complementary relaxation condition (60e), when $g_1^2+g_2^2-P<0$ we can obtain $\lambda=0$, and hence with (60c) and (60d) the optimal solution can be derived as

$$g_1^\star=\frac{-v_1}{2a},\quad g_2^\star=\frac{-v_2}{2a}. \tag{61}$$

On the other hand, if $g_1^2+g_2^2-P=0$, λ will be a positive number such that the optimal solution under this case is

$$g_1^{opt}=\frac{-v_1}{2a+2\lambda},\quad g_2^{opt}=\frac{-v_2}{2a+2\lambda}. \tag{62}$$

Furthermore, combining $g_1^2+g_2^2-P=0$ and (62), we can get an implicit expression of λ as $2a+2\lambda=\sqrt{\frac{v_1^2+v_2^2}{P}}$, and then (62) can be rewritten as

$$g_1^{opt}=\frac{-(v_1/(2a))\sqrt{P}}{\sqrt{(v_1/(2a))^2+(v_2/(2a))^2}}=\frac{g_1^\star\sqrt{P}}{\sqrt{(g_1^\star)^2+(g_2^\star)^2}}, \tag{63}$$

$$g_2^{opt}=\frac{-(v_2/(2a))\sqrt{P}}{\sqrt{(v_1/(2a))^2+(v_2/(2a))^2}}=\frac{g_2^\star\sqrt{P}}{\sqrt{(g_1^\star)^2+(g_2^\star)^2}}. \tag{64}$$

The above descriptions indicate that, the critical point $\{g_1^\star,g_2^\star\}$ of unconstrained problem $\min_{g_1,g_2}I(g_1,g_2)$ can be exploited to express the optimal solution of (62). Specifically, when $(g_1^\star)^2+(g_2^\star)^2<P$ (i.e., $\lambda=0$), $\{g_1^\star,g_2^\star\}$ is the optimal solution of the original problem (58). However, in the case of $(g_1^\star)^2+(g_2^\star)^2>P$ (i.e., $\lambda>0$), $\{g_1^\star,g_2^\star\}$ is not the optimal point since it violates constraint, but by employing the methods in (63) and (64) we can obtain the optimal solution $\{g_1^{opt},g_2^{opt}\}$ satisfying $(g_1^{opt})^2+(g_2^{opt})^2=P$. Moreover, regarding the

expression $\mathbf{z}_{i,j} = [z_{i,2j-1},\ z_{i,2j},\ z_{i,2j+1}]^T$, it is trivial to show that the above conclusions on problem (58) still hold.

Subsequently, considering the independence of different subproblems $\min_{\mathbf{z}_{i,j}\in\hat{\chi}_{i,j}} f(\mathbf{z}_{i,j})$, we can directly extend the closed-form expressions (61), (63), and (64) to the problem $\min_{\mathbf{z}_i\in\chi_i} f(\mathbf{z}_i)$, i.e., combining these closed-form expressions into a more compact manner. To be more specific, the combination of (61) for all entries in $\mathbf{z}_i$ results in equation (34), and the combination of (63) and (64) results in equation (35) by letting $g_1^\star = z_{i,l}^\star$ and $g_2^\star = z_{i,l+1}^\star$. Hence, we conclude the proof. ■

REFERENCES

[1] S. Yang and L. Hanzo, "Fifty Years of MIMO Detection: The Road to Large-Scale MIMOs," *IEEE Communications Surveys & Tutorials*, vol. 17, no. 4, pp. 1941–1988, Fourthquarter 2015.

[2] M. Costa, "Writing on Dirty Paper," *IEEE Transactions on Information Theory*, vol. 29, no. 3, pp. 439–441, May 1983.

[3] G. Caire and S. Shamai, "On the Achievable Throughput of a Multiantenna Gaussian Broadcast Channel," *IEEE Transactions on Information Theory*, vol. 49, no. 7, pp. 1691–1706, July 2003.

[4] R. Wesel and J. Cioffi, "Achievable Rates for Tomlinson-Harashima Precoding," *IEEE Transactions on Information Theory*, vol. 44, no. 2, pp. 824–831, Mar. 1998.

[5] L. Sun and M. Lei, "Quantized CSI-Based Tomlinson-Harashima Precoding in Multiuser MIMO Systems," *IEEE Transactions on Wireless Communications*, vol. 12, no. 3, pp. 1118–1126, Mar. 2013.

[6] B. Hochwald, C. Peel, and A. Swindlehurst, "A Vector-Perturbation Technique for Near-Capacity Multiantenna Multiuser Communication-Part II: Perturbation," *IEEE Transactions on Communications*, vol. 53, no. 3, pp. 537–544, Mar. 2005.

[7] T. Lo, "Maximum Ratio Transmission," *IEEE Transactions on Communications*, vol. 47, no. 10, pp. 1458–1461, Oct. 1999.

[8] A. Wiesel, Y. C. Eldar, and S. Shamai, "Zero-Forcing Precoding and Generalized Inverses," *IEEE Transactions on Signal Processing*, vol. 56, no. 9, pp. 4409–4418, Sep. 2008.

[9] C. Peel, B. Hochwald, and A. Swindlehurst, "A Vector-Perturbation Technique for Near-Capacity Multiantenna Multiuser Communication-Part I: Channel Inversion and Regularization," *IEEE Transactions on Communications*, vol. 53, no. 1, pp. 195–202, Jan. 2005.

[10] M. Bengtsson and B. Ottersten, "Optimal Downlink Beamforming Using Semidefinite Optimization," pp. 987–996, Sep. 1999.

[11] M. Schubert and H. Boche, "Solution of the Multiuser Downlink Beamforming Problem With Individual SINR Constraints," *IEEE Transactions on Vehicular Technology*, vol. 53, no. 1, pp. 18–28, Jan. 2004.

[12] A. Wiesel, Y. Eldar, and S. Shamai, "Linear Precoding via Conic Optimization for Fixed MIMO Receivers," *IEEE Transactions on Signal Processing*, vol. 54, no. 1, pp. 161–176, Jan. 2006.

[13] A. Li, D. Spano, J. Krivochiza, S. Domouchtsidis, C. G. Tsinos, C. Masouros, S. Chatzinotas, Y. Li, B. Vucetic, and B. Ottersten, "A Tutorial on Interference Exploitation via Symbol-Level Precoding: Overview, State-of-the-Art and Future Directions," *IEEE Communications Surveys & Tutorials*, vol. 22, no. 2, pp. 796–839, Secondquarter 2020.

[14] C. Masouros, T. Ratnarajah, M. Sellathurai, C. B. Papadias, and A. K. Shukla, "Known Interference in the Cellular Downlink: A Performance Limiting Factor or a Source of Green Signal Power?" *IEEE Communications Magazine*, vol. 51, no. 10, pp. 162–171, Oct. 2013.

[15] G. Zheng, I. Krikidis, C. Masouros, S. Timotheou, D.-A. Toumpakaris, and Z. Ding, "Rethinking the Role of Interference in Wireless Networks," *IEEE Communications Magazine*, vol. 52, no. 11, pp. 152–158, Nov. 2014.

[16] C. Masouros and E. Alsusa, "A Novel Transmitter-Based Selective-Precoding Technique for DS/CDMA Systems," *IEEE Signal Processing Letters*, vol. 14, no. 9, pp. 637–640, Sep. 2007.

[17] C. Masouros and E. Alsusa, "Dynamic Linear Precoding for the Exploitation of Known Interference in MIMO Broadcast Systems," *IEEE Transactions on Wireless Communications*, vol. 8, no. 3, pp. 1396–1404, Mar. 2009.

[18] C. Masouros, "Correlation Rotation Linear Precoding for MIMO Broadcast Communications," *IEEE Transactions on Signal Processing*, vol. 59, no. 1, pp. 252–262, Jan. 2011.

[19] C. Masouros and G. Zheng, "Exploiting Known Interference as Green Signal Power for Downlink Beamforming Optimization," *IEEE Transactions on Signal Processing*, vol. 63, no. 14, pp. 3628–3640, July 2015.

[20] M. Alodeh, S. Chatzinotas, and B. Ottersten, "Symbol-Level Multiuser MISO Precoding for Multi-Level Adaptive Modulation," *IEEE Transactions on Wireless Communications*, vol. 16, no. 8, pp. 5511–5524, Aug. 2017.

[21] A. Haqiqatnejad, F. Kayhan, and B. Ottersten, "Power Minimizer Symbol-Level Precoding: A Closed-Form Suboptimal Solution," *IEEE Signal Processing Letters*, vol. 25, no. 11, pp. 1730–1734, Nov. 2018.

[22] J. Yang, A. Li, X. Liao, and C. Masouros, "Low Complexity SLP: An Inversion-Free, Parallelizable ADMM Approach," *IEEE Transactions on Wireless Communications*, vol. 23, no. 9, pp. 12 424–12 439, Sep. 2024.

[23] A. Li and C. Masouros, "Interference Exploitation Precoding Made Practical: Optimal Closed-Form Solutions for PSK Modulations," *IEEE Transactions on Wireless Communications*, vol. 17, no. 11, pp. 7661–7676, Nov. 2018.

[24] A. Li, C. Masouros, B. Vucetic, Y. Li, and A. L. Swindlehurst, "Interference Exploitation Precoding for Multi-Level Modulations: Closed-Form Solutions," *IEEE Transactions on Communications*, vol. 69, no. 1, pp. 291–308, Jan. 2021.

[25] A. Li, C. Shen, X. Liao, C. Masouros, and A. Lee Swindlehurst, "Practical Interference Exploitation Precoding Without Symbol-by-Symbol Optimization: A Block-Level Approach," *IEEE Transactions on Wireless Communications*, vol. 22, no. 6, pp. 3982–3996, June 2023.

[26] J. Yang, A. Li, X. Liao, and C. Masouros, "Speeding-Up Symbol-Level Precoding Using Separable and Dual Optimizations," *IEEE Transactions on Communications*, vol. 71, no. 12, pp. 7056–7071, Dec. 2023.

[27] A. Mohammad, C. Masouros, and Y. Andreopoulos, "Learning-Based Symbol Level Precoding: A Memory-Efficient Unsupervised Learning Approach," pp. 429–434, Apr. 2022.

[28] F. Sohrabi, H. V. Cheng, and W. Yu, "Robust Symbol-Level Precoding via Autoencoder-Based Deep Learning," pp. 8951–8955, May 2020.

[29] Z. Bo, R. Liu, M. Li, and Q. Liu, "Deep Learning Based Efficient Symbol-Level Precoding Design for MU-MISO Systems," *IEEE Transactions on Vehicular Technology*, vol. 70, no. 8, pp. 8309–8313, Aug. 2021.

[30] B. Li, H. H. Dam, K. L. Teo, and A. Cantoni, "A Survey on Zero-Forcing Beamformer Design Under Per-Antenna Power Constraints for Multiuser MIMO Systems," pp. 329–333, July 2015.

[31] J. Choi, S. Han, and J. Joung, "Low-Complexity Multiuser MIMO Precoder Design Under Per-Antenna Power Constraints," *IEEE Transactions on Vehicular Technology*, vol. 67, no. 9, pp. 9011–9015, Sep. 2018.

[32] W. Yu and T. Lan, "Transmitter Optimization for the Multi-Antenna Downlink With Per-Antenna Power Constraints," *IEEE Transactions on Signal Processing*, vol. 55, no. 6, pp. 2646–2660, June 2007.

[33] D. Spano, M. Alodeh, S. Chatzinotas, and B. Ottersten, "Per-Antenna Power Minimization in Symbol-Level Precoding," in *2016 IEEE Global Communications Conference (GLOBECOM)*, Dec. 2016, pp. 1–6.

[34] D. Spano, S. Chatzinotas, J. Krause, and B. Ottersten, "Symbol-Level Precoding With Per-Antenna Power Constraints for the Multi-Beam Satellite Downlink," in *2016 8th Advanced Satellite Multimedia Systems Conference and the 14th Signal Processing for Space Communications Workshop (ASMS/SPSC)*, Sep. 2016, pp. 1–8.

[35] D. Spano, M. Alodeh, S. Chatzinotas, and B. Ottersten, "Symbol-Level Precoding for the Nonlinear Multiuser MISO Downlink Channel," *IEEE Transactions on Signal Processing*, vol. 66, no. 5, pp. 1331–1345, Mar. 2018.

[36] C.-E. Chen, "Computationally Efficient Constructive Interference Precoding for PSK Modulations Under Per-Antenna Power Constraint," *IEEE Transactions on Vehicular Technology*, vol. 69, no. 8, pp. 9206–9211, Aug. 2020.

[37] Y. Wen, H. Wang, A. Li, X. Liao, and C. Masouros, "Low-Complexity Interference Exploitation MISO Precoding Under Per-Antenna Power Constraint," *IEEE Transactions on Wireless Communications*, vol. 23, no. 8, pp. 9943–9957, Aug. 2024.

[38] W. Deng, M. J. Lai, Z. Peng, and W. Yin, "Parallel Multi-Block ADMM with o(1 / k) Convergence," *Journal of Scientific Computing*, vol. 71, no. 2, pp. 712–736, Jan. 2017.

[39] Bingsheng, He, Liusheng, Hou, Xiaoming, and Yuan, "On Full Jacobian Decomposition of the Augmented Lagrangian Method for Separable Convex Programming," *SIAM Journal on Optimization*, vol. 25, no. 4, pp. 2274–2312, Mar. 2014.

[40] B. He, H. K. Xu, and X. Yuan, "On the Proximal Jacobian Decomposition of ALM for Multiple-Block Separable Convex Minimization

Problems and Its Relationship to ADMM," *Journal of Scientific Computing*, vol. 66, no. 3, pp. 1204–1217, June 2015.

[41] R. Hunger, "Floating Point Operations in Matrix-Vector Calculus," Oct. 2005.

[42] E. S. P. Lopes and L. T. N. Landau, "MMSE Symbol Level Precoding Under a Per Antenna Power Constraint for Multiuser MIMO Systems With PSK Modulation," *IEEE Wireless Communications Letters*, vol. 11, no. 11, pp. 2440–2444, Nov. 2022.

Yunsi Wen (S'23) received the B.S. degree in communication engineering from Northwestern Polytechnical University in 2022. He is currently pursuing the M.S. degree with the School of Information and Communications Engineering, Faculty of Electronic and Information Engineering, Xi'an Jiaotong University. His research interests include Symbol-Level Precoding and Physical-Layer Optimization.

Junwen Yang (S'23) received the B.S. degree in electronic information engineering and the M.S. degree in electronic and communication engineering from Central China Normal University, Wuhan, China, in 2017 and 2019, respectively. He is working toward the Ph.D. degree with the School of Information and Communications Engineering, Xi'an Jiaotong University, Xi'an, China. His current research interests mainly focus on wireless communications, signal processing, optimizations, and symbol-level precoding.

Ang Li (S'14-M'18-SM'21) received his Ph.D. degree in the Communications and Information Systems research group, Department of Electrical and Electronic Engineering, University College London in April 2018. He was a postdoctoral research associate in the School of Electrical and Information Engineering, The University of Sydney from May 2018 to February 2020. He joined Xi'an Jiaotong University in March 2020 and is now a Professor in the School of Information and Communications Engineering, Faculty of Electronic and Information Engineering, Xi'an Jiaotong University, Xi'an, China. His main research interests lie in the physical-layer techniques in wireless communications, including MIMO/massive MIMO, interference exploitation, symbol-level precoding, and reconfigurable MIMO, etc. He currently serves as the Associate Editor for IEEE Communications Letters, IEEE Open Journal of Signal Processing, and EURASIP Journal on Wireless Communications and Networking. He is the recipient of the 2021 IEEE Signal Processing Society Young Author Best Paper Award. He has been an Exemplary Reviewer for IEEE Communications Letters, IEEE Transactions on Communications, and IEEE Wireless Communications Letters. He has served as the Co-Chair of the IEEE ICASSP 2020 Special Session on 'Hardware-Efficient Large-Scale Antenna Arrays: The Stage for Symbol-Level Precoding', and has organized a Tutorial in IEEE ICC 2021 on 'Interference Exploitation through Symbol Level Precoding: Energy Efficient Transmission for 6G and Beyond'.

Xuewen Liao received the B.S. and Ph.D. degrees in information and communications engineering from Xi'an Jiaotong University, Xi'an, China, in 2002 and 2008, respectively. From 2008 to 2012, he was an Assistant Professor at Xi'an Jiaotong University. From 2016 to 2017, he was a Visiting Scholar at the Department of Electrical and Computer Engineering, The University of British Columbia, Vancouver, BC, Canada. He is currently a Professor with the School of Information and Communications Engineering, Xi'an Jiaotong University. His research interests include wireless energy transfer, green communications, relay communications, and indoor positioning.

Christos Masouros (Fellow, IEEE) received the Diploma degree in Electrical and Computer Engineering from the University of Patras, Greece, in 2004, and MSc by research and PhD in Electrical and Electronic Engineering from the University of Manchester, UK in 2006 and 2009 respectively. In 2008 he was a research intern at Philips Research Labs, UK, working on the LTE standards. Between 2009-2010 he was a Research Associate in the University of Manchester and between 2010-2012 a Research Fellow in Queens University Belfast. In 2012 he joined University College London as a Lecturer. He has held a Royal Academy of Engineering Research Fellowship between 2011-2016. Since 2019 he is a Full Professor of Signal Processing and Wireless Communications in the Information and Communication Engineering research group, Dept. Electrical and Electronic Engineering, and affiliated with the Institute for Communications and Connected Systems, University College London. His research interests lie in the field of wireless communications and signal processing with particular focus on Green Communications, Large Scale Antenna Systems, Integrated Sensing and Communications, interference mitigation techniques for MIMO and multicarrier communications.